Ore Geology Reviews 80 (2017) 214–228

Contents lists available at ScienceDirect

Ore Geology Reviews

journal homepage: www.elsevier.com/locate/oregeorev

Fluid inclusion and stable isotopic constraints on fluid sources and evolution of the Luojiahe Cu deposit in the southern margin of the North China Craton

Yuhang Jiang [a,b], Hecai Niu [a,*], Yan Zhao [a,b], Zhiwei Bao [a], Ningbo Li [a,b], Qiang Shan [a]

[a] Key Laboratory of Mineralogy and Metallogeny, Guangzhou Institute of Geochemistry, Chinese Academy of Sciences, Guangzhou 510640, China
[b] University of Chinese Academy of Sciences, Beijing 100049, China

ARTICLE INFO

Article history:
Received 4 January 2016
Received in revised form 23 June 2016
Accepted 26 June 2016
Available online 2 July 2016

Keywords:
Luojiahe Cu deposit
North China Craton
Neoarchean VMS
CH_4-rich metamorphic fluids
C-H-O isotopes

ABSTRACT

The Luojiahe Cu deposit in the Zhongtiaoshan region is located in the southern margin of the North China Craton. The orebodies are hosted in the mafic volcanic-sedimentary sequences of the metamorphosed (greenschist-facies) Neoarchean Songjiashan Group. The Luojiahe Cu mineralization can be divided into the primary volcanogenic massive sulfide (VMS) mineralization stage (Stage I, banded or stockwork ores) and the subsequent metamorphic remobilization stage (Stage II, coarse-vein ores).

Three types of quartz selected for fluid inclusion (FI) studies were collected from the Stage I banded (Q1) and stockwork (Q2) ores and Stage II coarse-vein (Q3) ores. Four types of FIs were identified: (1) liquid-rich FIs (L-type), (2) pure vapor and vapor-rich FIs (V-type), (3) daughter mineral-bearing FIs (S-type), and (4) CH_4-H_2O FIs (C-type). Systematical microthermometric and H-O isotopic studies show that the Stage I ore-forming fluids consist predominantly of high salinity evolved seawater (125–220 °C; 23.9–27.9 wt.% NaCl equiv.) and some magmatic-hydrothermal fluids (249–339 °C; 34.5–42.2 wt.% NaCl equiv.). The two fluid end-members are represented by the L-type FIs in Q1 and the S- and V-type FIs in Q2. The temperature- and salinity variation trends of the L-type FIs in Q1 indicate a mixing process between the hot evolved seawater and cold seawater at Stage I. Furthermore, the V- and S-type FI coexistence in Q2 and their microthermometric data suggest that fluid unmixing has occurred in original magmatic fluids at Stage I. In contrast, the Stage II ore-forming fluids consist of CH_4-rich metamorphic fluids (192–350 °C; 10.6–43.2 wt.% NaCl equiv.). Carbon isotopic analysis of the Stage II calcite (−4.58 to −10.83‰) and graphite (−32.01 to −39.16‰) in the ore-hosting chlorite schist indicates that the metamorphic ore-forming fluids had exchanged carbon isotope with graphite. The generation of CH_4 may have resulted from the interaction between H_2O (released by metamorphic devolatilization) and graphite. The continuous consumption of H_2O in the hydrothermal fluid system may have increased the fluid salinity and triggered fluid unmixing in the CH_4-NaCl-H_2O system. In addition, the VMS metallogenic environment is generally favorable for microbial communities. It is considered that the graphite at Luojiahe may have been derived from sedimentary organic matter formed in seafloor hydrothermal vent systems, as also supported by carbon isotopic data. We propose that at Stage I, the main mineralization may have been resulted from 1) fluid mixing of hot evolved seawater and cold seawater in the near-surface environment; and 2) fluid unmixing caused by the percolation of magmatic fluids into syn-volcanic faults, forming the stockwork ores. At Stage II, the interaction between H_2O and graphite may have resulted in the reduction of ore-forming fluids and Cu precipitation, and fluid unmixing in the CH_4-NaCl-H_2O system may have further promoted the Cu mineralization.

1. Introduction

Since the first discovery of active hydrothermal vents at the Galapagos Rift in 1977 (Corliss et al., 1979), the study on ore-forming fluids of volcanogenic massive sulfide deposits (VMS) has expanded (Ripley and Ohmoto, 1977; Spooner and Bray, 1977; de Ronde, 1995; Bodnar et al., 2014). Fluid inclusions (FIs) trapped in hydrothermal minerals provide the best available way for constraining the physical and chemical conditions of ore-forming fluids in fossilized hydrothermal systems (Bodnar et al., 2014). By comparing the modern vent fluid data with FI data from fossilized hydrothermal systems, the compositions and physical nature of the ore-forming fluids, VMS mineralization

* Corresponding author.
E-mail address: niuhc@gig.ac.cn (H. Niu).

http://dx.doi.org/10.1016/j.oregeorev.2016.06.028
0169-1368/

processes and secular changes of seawater compositions throughout the Earth's history, are becoming better documented (e.g., Ohmoto et al., 1983; de Ronde, 1995; de Ronde et al., 1997; Franklin et al., 2005; Huston et al., 2010; Bodnar et al., 2014).

The Archean greenstone-hosted VMS deposits are the oldest VMS deposits and account for ca. 8% of the global VMS-hosted metal resource (Mercier-Langevin et al., 2014). However, FI studies on these ancient VMS deposits are still rare (de Ronde et al., 1997; Bodnar et al., 2014), because most of these deposits were remobilized by subsequent metamorphism (Marshall and Gilligan, 1993; Tornos et al., 2015). The origin of the ore-forming fluids entrapped in the VMS deposits is highly controversial (Ripley and Ohmoto, 1977; Broman, 1987; Hall, 1989; Giles and Marshall, 1994; de Ronde et al., 1997; Lowe and Byerly, 2003; Moura, 2005; Bradshaw et al., 2008; Xu et al., 2011), especially regarding the preservation of primary FIs, sources of metamorphic carbonic fluids (CO_2 or CH_4), and the roles of both primary vent fluids and metamorphic hydrothermal fluid systems in the mineralization (Xu et al., 2011).

The Luojiahe Cu deposit is hosted in the Archean greenstone terranes in the Zhongtiaoshan region (hereafter referred to as ZTS), in the southern margin of the North China Craton (Li, 1986). This deposit was argued to be a Neoarchean VMS deposit that was subsequently modified by deformation and metamorphism during the Zhongtiao Movement (ca. 1.85 Ga) (Zhen and Xi, 1990; Zhen et al., 1993; Huang et al., 2001; Jiang et al., 2013). Detailed FI study is essential to constrain the origin and evolution of the Luojiahe ore-forming fluids. In this paper, based on detailed field and petrographic observations and FI analyses, we identified primary FIs in the banded VMS ores and first detected significant CH_4 in the hydrothermal quartz veins of the metamorphic mineralization stage. The fluid sources and evolution of the two metallogenic stages were discussed on the basis of FI systematics and C-H-O isotopes. Our study also provides new insight into the understanding of the original submarine hydrothermal processes and the possible role of CH_4 in the metamorphic overprinting on the Archean VMS deposits.

2. Regional geology

The ZTS is located in the southern segment of the Trans-North China Orogen (Fig. 1A), along which the discrete Eastern and Western Blocks amalgamated to form the North China Craton (Zhao et al., 2001, 2002a; Liu et al., 2012). The Neoarchean to the Late Paleoproterozoic ZTS ore deposits contain a total endowment of ca. 400 Mt. Cu metal (Xu, 2010). Archean rock units in this region consist mainly of low-grade granite-greenstone terranes (2.7–2.5 Ga), including granitoids (Sushui complex) and meta-mafic volcanic-sedimentary sequences (Songjiashan Group) (Sun and Hu, 1993; Feng and Wang, 2008; Zhao et al., 2008; Liu et al., 2012). Paleoproterozoic rock units include (from the oldest to the youngest) the Jiangxian (2.2–2.1 Ga), Zhongtiao (2.06–1.9 Ga) and Danshanshi Groups (~1.85 Ga) (Sun and Hu, 1993; Bai, 1997; Zhen and Wu, 2007; Liu et al., 2012; Fig. 1B). They contain mainly schist and quartzite, with variable amount of intercalated carbonates and metavolcanic rocks (Bai, 1997; Liu et al., 2012). These rock units had experienced greenschist- to low amphibolite-facies metamorphism led by the Eastern and Western Blocks collision (~1.85 Ga) (Liu et al., 2012), and are unconformably overlain by the unmetamorphosed Xiyanghe Group andesitic volcanic rocks (~1.78 Ga) (Chen et al., 1992; Zhao et al., 2002b; He et al., 2009), which is widely exposed in the eastern ZTS (Fig. 1B). The Songjiashan Group, exposed as several inliers (such as Tongshan, Wangwu, Luojiahe inliers) within the overlying Xiyanghe Group (Fig. 1B), is the host of the Luojiahe and Huping Cu deposits.

The ZTS is extensively deformed, with the basement-cutting SE- or SW-trending faults being the host structures of many stratiform Cu deposits, e.g., at Luojiahe, Huping, Tongkuangyu, Hujiayu and Bizigou (Sun et al., 1995; Fig.1B).

3. Ore deposit geology

3.1. Wall rocks

The Luojiahe Cu deposit is hosted in metamorphosed mafic volcanic-sedimentary rocks of the Neoarchean Songjiashan Group,

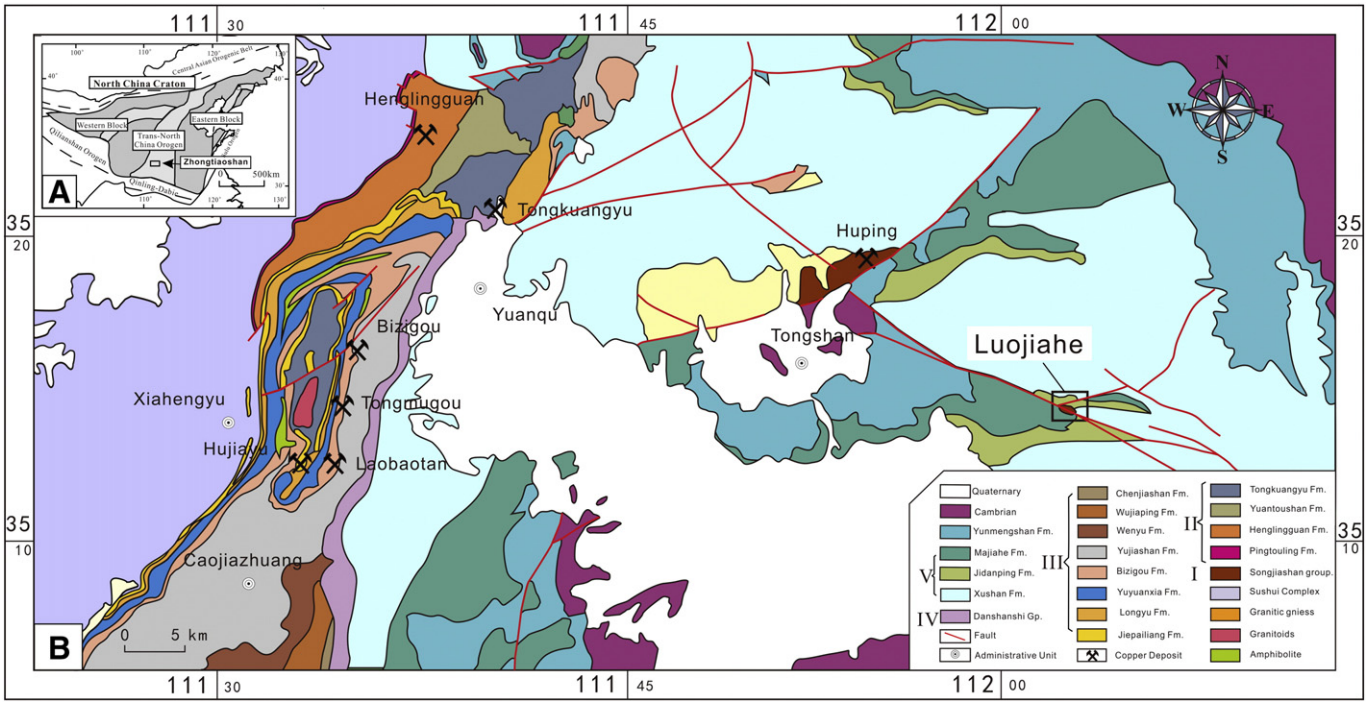

Fig. 1. Regional geological map of the Zhongtiaoshan area. (A). Tectonic framework of the North China Craton and the location of Zhongtiaoshan (modified after Zhao et al., 2001). (B). Regional geology of the Zhongtiaoshan area. I-Songjiashan Group; II-Jiangxian Group; III-Zhongtiao Group; IV-Dashanshi Group; V-Xiyanghe Group (modified after Sun and Hu, 1993).

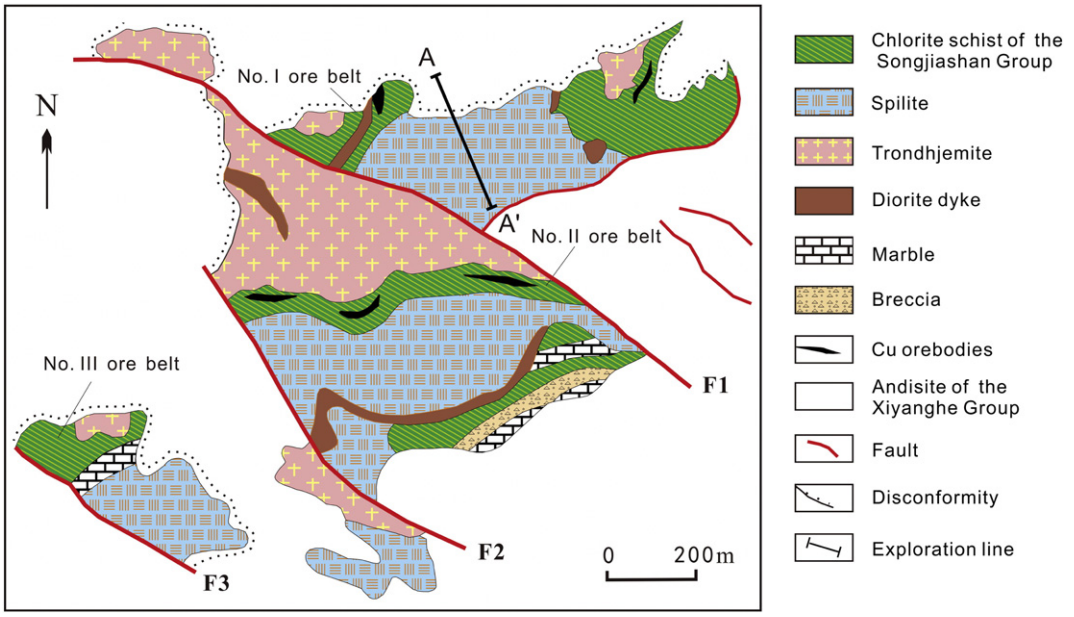

Fig. 2. Geological map of the Luojiahe Cu deposit (modified after Zhen et al., 1993).

which is exposed in the inliers of the younger andesite of the Xiyanghe Group (Gu et al., 1993; Sun and Hu, 1993; Fig. 2). The Songjiashan Group at Luojiahe consists of chlorite schist, spilite and marble (Figs. 3, 4B, and C). The major orebodies are hosted in graphite-bearing chlorite schist. At Luojiahe, trondhjemite (zircon U-Pb: 2471 ± 25 Ma; Zhao et al., 2016) was widely found intruding into the lowermost spilites and chlorite schist (Figs. 3, 4A, and D).

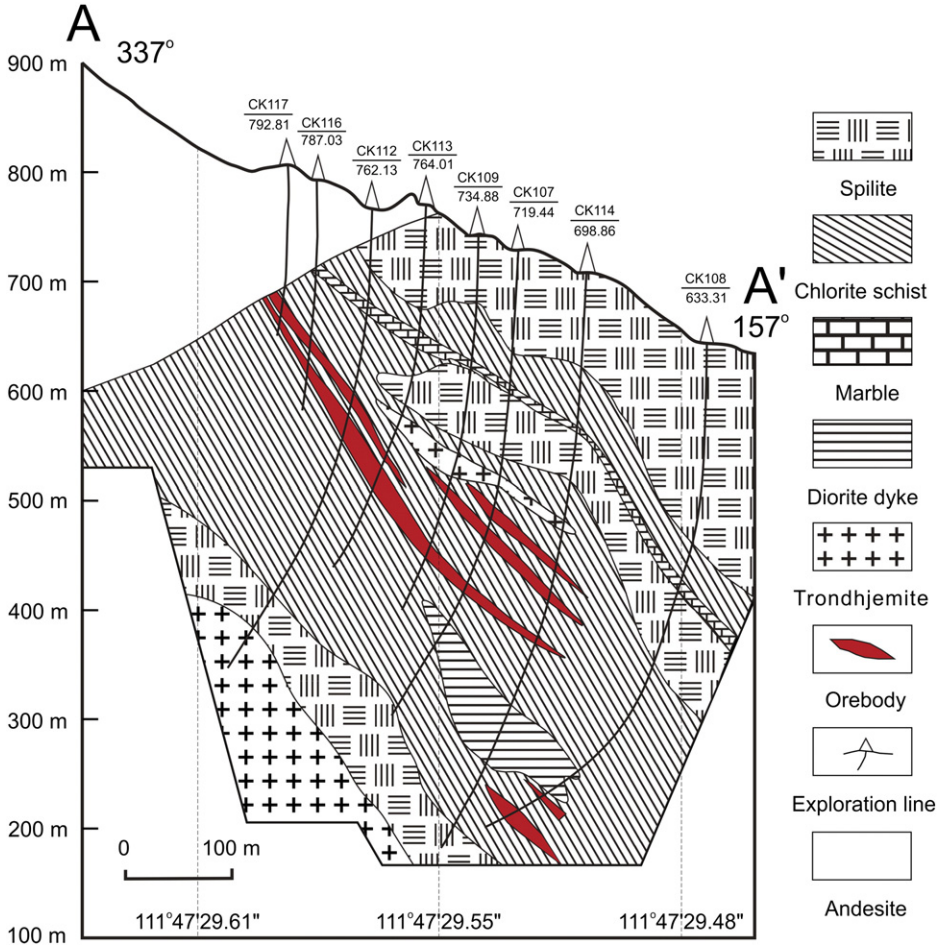

Fig. 3. Geological profile of the Luojiahe No. 1 exploration line (modified after Zhen et al., 1993).

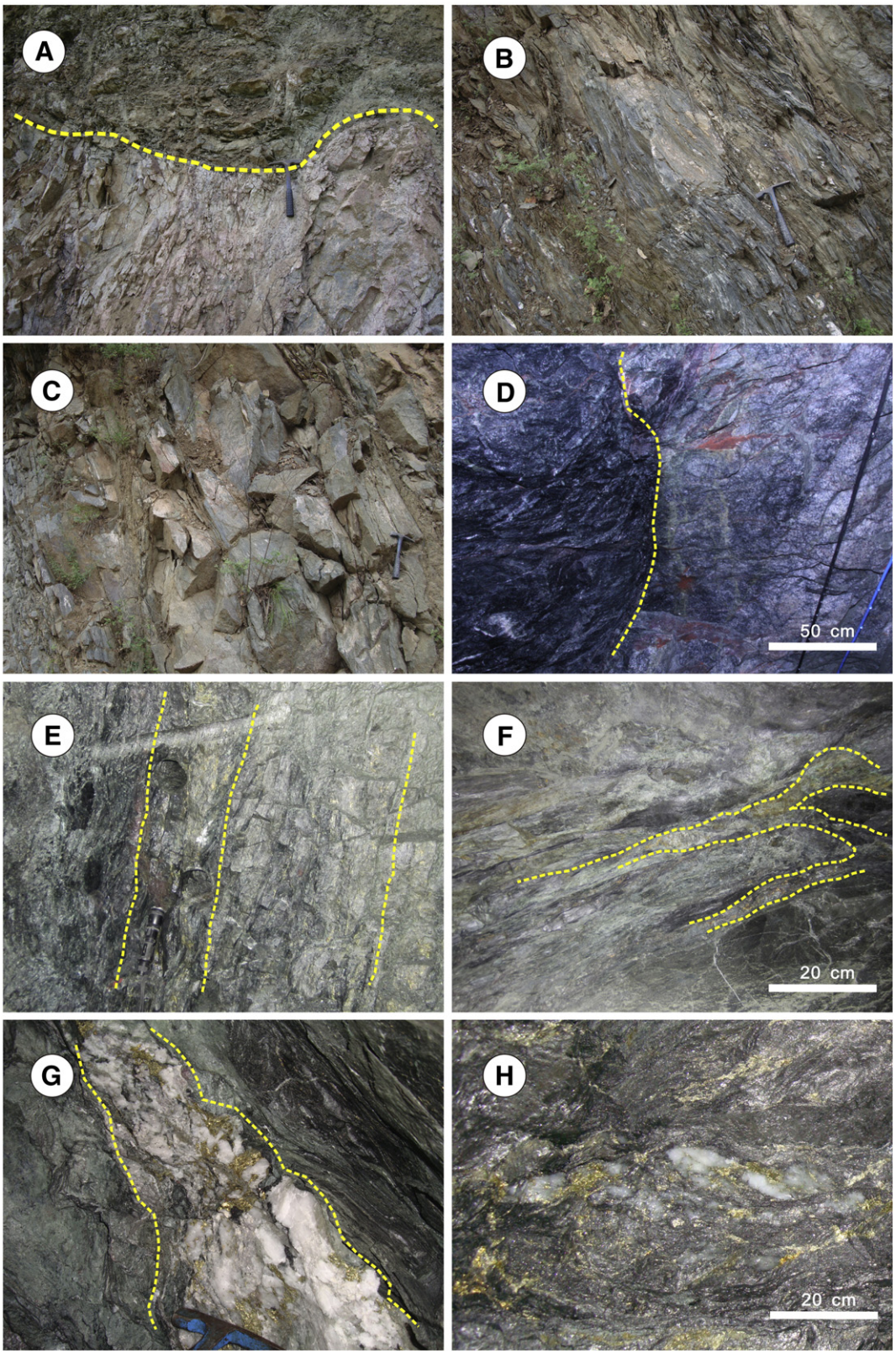

Fig. 4. Field photos of the Luojiahe Cu mineralization and host rocks: (A). Trondhjemite intruded the Songjiashan Group chlorite schist. (B). The Songjiashan Group chlorite schist (C). The Songjiashan Group spilite. (D). Trondhjemite intruded the splite below the orebodies. (E). Stage I banded mineralization in the chlorite schist. (F). Stage I stockwork ores in the lower orebodies. (G) and (H) Stage II thick ore-bearing quartz veins crosscut the graphite-bearing chlorite schist.

3.2. Structures

The regional SE-trending normal fault were suggested to have uplifted and exposed the Songjiashan Group rocks at Luojiahe, which are in turn crosscut by three SE-trending parallel faults (namely the F1, F2, and F3) (Fig. 2). The wave-like ductile shears related to the later faulting in the chlorite schist control most of the ore body emplacement.

3.3. Orebodies

The Luojiahe Cu deposit (resource: 260,000 t Cu metal @ 1.11% Cu (average grade) (Zhen et al., 1993) conain three ore belts, i.e., the No. I (Yingziling), No. II (Yangshukeng) and No. III (Huituao) (Zhen et al., 1993; Huang et al., 2001; Fig. 2). The orebodies are commonly stratabound lensoidal in shape. Ore Belt No. I contain 57 orebodies, among which the largest Orebody No. 1 (800 m long, 750 m wide and 14 m thick) has an average Cu grade of 1.09% and accounts for 83.7% of the ore belt's metal reserve. Ore Belt No. II contains six orebodies, among which Orebody No. 25 (420 m long, 600 m wide and 22.5 m thick) has an average Cu grade of 1.07% and accounts for 94% of the ore belt's reserve. Only Ore Belt No. I is now in operation, whereas the other two are still under exploration.

3.4. Mineralization and alteration

The wall rocks of the Luojiahe Cu deposit were extensively altered and contain various secondary minerals, e.g., chlorite (dominant), quartz, sericite, calcite, albite, graphite and tourmaline. The intense chlorite alteration had obliterated much of the original wall rock textures. The alteration sequence and zonation are unclear, partly attributed to the intense regional metamorphic overprinting (Zhen et al., 1993).

The mineralization observed in the Luojiahe copper deposit can be divided into the primary VMS stage (Stage I) and the secondary metamorphic remobilization stage (Stage II):

Stage I mineralization is characterized by disseminated-, banded-, massive- and stockwork sulfides in chlorite schist (Fig. 4E). Metallic minerals include mainly chalcopyrite and pyrite with accessory sphalerite, bornite and minor cobaltite. Non-metallic minerals include mainly quartz, calcite, albite and tourmaline (Mg-Fe-series). In the banded ores, the quartz-sulfide veinlets (<0.8 cm wide) and chlorite schists occur at interbedding (Fig. 5A). Tourmaline is locally present as isolated euhedral grains in chalcopyrite-quartz veinlets (Fig. 5B). The stockwork ores, occurring in the lower orebodies, have irregular boundaries with the host rocks (Figs. 4F and 5C).

Stage II mineralization is characterized by more continuous and thicker (2 to 50 cm wide) sulfide-quartz-calcite veins (cf. the Stage I ones) (Fig. 4G and H), which contain chalcopyrite, pyrite, pyrrhotite, bornite, sphalerite, quartz and calcite (Fig. 5D). Quartz in the veins occurs as coarse-grained aggregate and coexists with chalcopyrite (Fig. 5E and F). Exsolution (among chalcopyrite and bornite) and emulsion (among chalcopyrite and sphalerite) textures are ubiquitous (Fig. 5H and I). Pyrite is replaced by chalcopyrite and occurs as islands in chalcopyrite (Fig. 5G). Different from Stage I, the Stage II mineralization is mainly hosted in graphite-rich chlorite schist, and the Stage II ore veins commonly crosscut the host rocks (Fig. 5F).

4. Sampling and analytical methods

4.1. Sample description

In this study, 120 samples were collected from the Exploration Tunnels No. 460 and No. 360 (in Orebody No. 1). Eighty-five (39 polished) thin sections were examined by transmitted- and reflected light microscopy. Fifty-five doubly polished sections for the different ore types were prepared for FI analyses, among which 25 were selected for microthermometry and laser Raman spectroscopy.

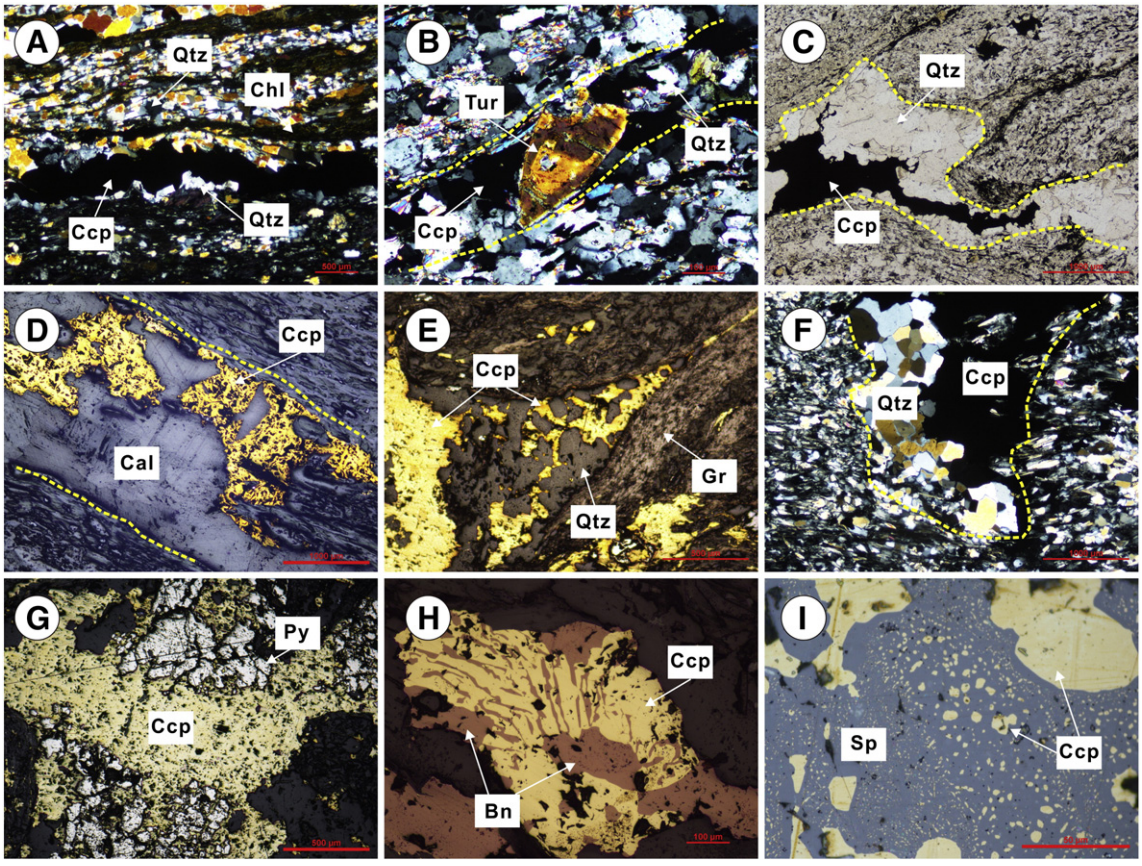

Fig. 5. Photomicrographs of the Luojiahe Cu ore textures and mineral assemblage: (A). Quartz-sulfide veinlets and chlorite schists occur at interbedding in the Stage I banded ores. (B). Euhedral zoned tourmaline in Stage I chalcopyrite-quartz veinlets. (C). Stage I barren-ore quartz stockwork in the lowest orebodies. (D). Stage II chalcopyrite-calcite veins crosscut the host rocks. (E) and (F). Stage II chalcopyrite-quartz veins crosscut graphite-bearing chlorite schist and chlorite schist, respectively. (G) Pyrite partially replaced by Stage II chalcopyrite. (H). Exsolution texture of chalcopyrite and bornite. (I) Emulsion texture of chalcopyrite and sphalerite. Abbreviations: Chl = chlorite; Qtz = quartz; Ccp = chalcopyrite; Tur = tourmarine; Cal = calcite; Gr = graphite; Py = pyrite; Bn = bornite; Sp = sphalerite.

Quartz samples were classified into three groups (Q1 to Q3) based on their field occurrence and morphological characteristics:

1) Q1 quartz is from the Stage I banded ores, and occurs as euhedral grains in chalcopyrite.
2) Q2 quartz is from the Stage I stockwork ores (Figs. 4F and 5C).
3) Q3 quartz is from the Stage II coarse sulfide-quartz-calcite veins (Fig. 5E and F).

Four Q2 and Q3 quartz samples were selected for the hydrogen and oxygen isotopic analyses. Detailed microscopic work was conducted to avoid the incorporation of secondary inclusions.

The calcite from the Stage II coarse sulfide-quartz-calcite veins was analyzed for its carbon and oxygen isotopic compositions. Four graphite samples from the graphite-rich chlorite schist were collected for the organic carbon isotope analysis.

4.2. Microthermometry

Microthermometry study was carried out using a Linkam TS 600 Heating-Freezing System at the Key Laboratory of Mineralogy and Metallogeny, Chinese Academy of Sciences (hereafter referred to as KLMMCAS). Thermocouples were calibrated at −196 to 600 °C using synthetic FIs. The precision of temperature measurement is ±0.1 °C between −100 and 25 °C, ± 1 °C between 25 and 400 °C, and ±2 °C above 400 °C. The heating rate was generally 0.2 to 5 °C/min during the analysis, but reduced to 0.1 °C/min near the freezing point, and 0.2 to 0.5 °C/min near the homogenization temperature to record the phase transformation process accurately.

4.3. Laser Raman microspectroscopy

Vapor and solid compositions of individual FIs were measured using the Horiba Xplora laser Raman microspectroscopy at KLMMCAS. An Ar^+ ion laser operating at 44 mW was used to produce an excitation wavelength of 532 nm line. The scanning range of spectra was set between 100 and 4000 cm^{-1} with an accumulation time of 10 s for each scan. The spectral resolution was 0.65 cm^{-1}. The Raman shift of a monocrystalline silicon piece was measured to be 520.7 cm^{-1} before the analysis.

4.4. Fluid inclusion references

Salinities of the halite daughter mineral-bearing FIs were estimated based on the temperatures of bubble dissolution and homogenization (Lecumberri-Sanchez et al., 2012). As for the FIs with eutectic temperatures below −21.2 °C (with the most of −52 °C), the fluid system is approximated by the H_2O-NaCl-$CaCl_2$ system. Salinities of these FIs were calculated by using the equations of Chi and Ni (2007). Salinities of the CH_4-rich FIs could not be calculated because no complete microthermometric data were acquired.

4.5. Carbon and oxygen isotopes

The calcite samples were crushed to 60 mesh and handpicked under a binocular microscope, and then crushed to 200 mesh for the measurement. Carbon and oxygen isotopic compositions were measured on an Isoprime 100 Isotopic Ratio Mass Spectrometer coupled with MultiFlow in KLMMCAS. About 0.1 mg powder sample was loaded in a sample vial and reacted with 100% H_3PO_4 at 90 °C for >2 h, then CO_2 was dried and measured by IRMS. Carbon and oxygen isotopic compositions were written to VPDB with unit of per mil, carbon and oxygen isotopic values were corrected by NBS19, the precisions were both better than 0.15 per mil.

The graphite was crushed to 200 mesh for organic carbon isotopic analyses. Carbon content and carbon isotopic composition in total organic carbon (TOC) were measured with an Isoprime 100 Isotopic Ratio Mass Spectrometer coupled with Pyro cube Elemental Analyzer in State Kay Lab of Isotope Geochemistry, GIG, CAS. Powder samples were loaded in a tin boat and combusted at 920 °C with flush O_2 and CuO, then CO_2 was dried and separated by column and measured by TCD and IRMS for carbon content and isotopic composition, respectively. Carbon isotopic compositions were written to VPDB with unit of per mil, whereas the carbon isotopic values were corrected by IAEA-CH3 and IAEA-CH7. The precision was 2% for TOC content and 0.15‰ for carbon isotopic composition, respectively.

4.6. Hydrogen and oxygen isotopes

Quartz grains were extracted from crushed and washed sample fragments, and purified by hand picking under a binocular microscope. The hydrogen and oxygen isotopes were analyzed on a Finnigan MAT253 mass spectrometer in the Analytical Laboratory, Beijing Research Institute of Uranium Geology. Oxygen was liberated from quartz by reaction with BrF_5 (Clayton et al., 1972) and converted to CO_2 on a platinum-coated carbon rod. Water from FIs in quartz was released by heating the samples in an induction furnace. Then the water would react with glassy carbon to generate hydrogen (Liu et al., 2013). All data were normalized with V-SMOW standards with analytical precisions better than ±0.2‰ and ±1‰ for $\delta^{18}O$ and δD, respectively.

5. Results

5.1. Fluid inclusion petrography

5.1.1. Fluid inclusion types

Primary FIs have generally negative crystal- or elliptical shapes, and occur in clusters or as isolated/randomly distributed FIs in quartz. Four primary FI types were identified based on their phases at room temperature (Roedder, 1984; Lu et al., 2004), phase transitions during total homogenization and laser Raman spectroscopy. These FI types were summarized in Table 1 and described in the following sections.

1) L-type (liquid-rich) FIs: They (5 to 23 μm in size) contain 10 to 35 vol.% vapor phases, with both the liquid- and vapor phases comprising primarily H_2O. They are commonly irregular or negative crystal in shape (Fig. 6A and G), occurring in clusters or scattered in quartz.
2) V-type (pure vapor or vapor-rich) FIs: They consist primarily of pure vapor (some with <30 vol.% liquid) and comprise mainly H_2O. They are mainly elliptical and range in size from 8 to 20 μm (Fig. 6C). V-type FIs are randomly distributed and coexist with S-type FIs (Fig. 6H).
3) S-type (daughter mineral-bearing) FIs: They occur in negative crystal or elliptical shapes, and contain 10 to 30 vol% of vapor. These FIs (5 to 30 μm in size) contain abundant daughter minerals, such as halite, sylvite, calcite and opaque minerals (Fig. 6B, E, H, and I). The FIs are distributed randomly or in clusters (Fig. 6H and I).
4) C-type (CH_4-rich) FIs: As identified by the Laser Raman spectroscopy and microthermometry, these FIs consist mainly of CH_4 vapor phase (>75% vol.%) and H_2O liquid phase. They are generally 5 to 25 μm in size and have negative crystal or elliptical shapes (Fig. 6F). These FIs occur as isolated FIs or in clusters (Fig. 6I), and commonly coexist with S-type FIs in Q3.

5.1.2. Occurrence and temporal relationship of fluid inclusions

Our study shows that the Stages I and II FIs are significantly different in their types, assemblages and compositions.

1) Q1: FIs in quartz from the banded ores are rare because most quartz was recrystallized during the subsequent deformation and metamorphism. However, Q1 from the banded ores remained unstrained because they are inside the sulfides (Fig. 7A and B). Systematic

Table 1
Overview of fluid inclusion types of the Luojiahe Cu deposit.

Type	Fluid phases	Daughter minerals	Size (μm)	Vol.%	Shape	Occurrence
L	$V_{H2O} + L_{H2O}$		5–23	10–35	Irregular or negative crystal	In clusters or scattered
V	V_{H2O} or $V_{H2O} + L_{H2O}$		8–20	>70	Elliptical	Randomly distributions
S	$V_{H2O} + L_{H2O}$	Halite, sylvite, calcite, opaque metal minerals	5–30	10–30	Negative crystal or elliptical	Randomly distributions or in clusters
C	V_{CH4} or $V_{CH4} + L_{H2O}$		5–25	>75	Negative crystal or elliptical	Isolated or in clusters

Abbreviations: V_{CH4}: CH_4 vapor; V_{H2O}: H_2O vapor; L_{H2O}: H_2O liquid; vol.%: the volume proportion of the vapor phase.

petrographic observation shows that L-type FIs, as disseminations or in clusters, are predominant in Q1 (Figs. 6G and 7C).

2) Q2: FIs are mainly of S- and V-type, which coexist mainly in clusters (Fig. 6H). Halite is the only daughter mineral identified.
3) Q3: The abundant FIs consist primarily of S- (dominant), C- and L-type. The daughter minerals identified include mainly halite, calcite and opaque minerals, with several daughter mineral types coexisting in one single S-type FI present in some occasions (Fig. 6E). C-type FIs are also widespread and commonly coexist with S-type FIs (Fig. 6I). L-type FIs occur in disseminations.

5.2. Microthermometric results

Results of the FI microthermometric analyses are listed in Table 2 and illustrated in Figs. 8 and 9. Microthermometric features of the various types of FIs were described below.

1) L-type FIs: They are highly common in both Stages I and II. For those in Q1 (Stage I), the eutectic temperatures range from −62.4 to −51 °C. Most of the data cluster around −52 °C, and thus the $CaCl_2$-NaCl-H_2O system was chosen to estimate the salinity (Oakes

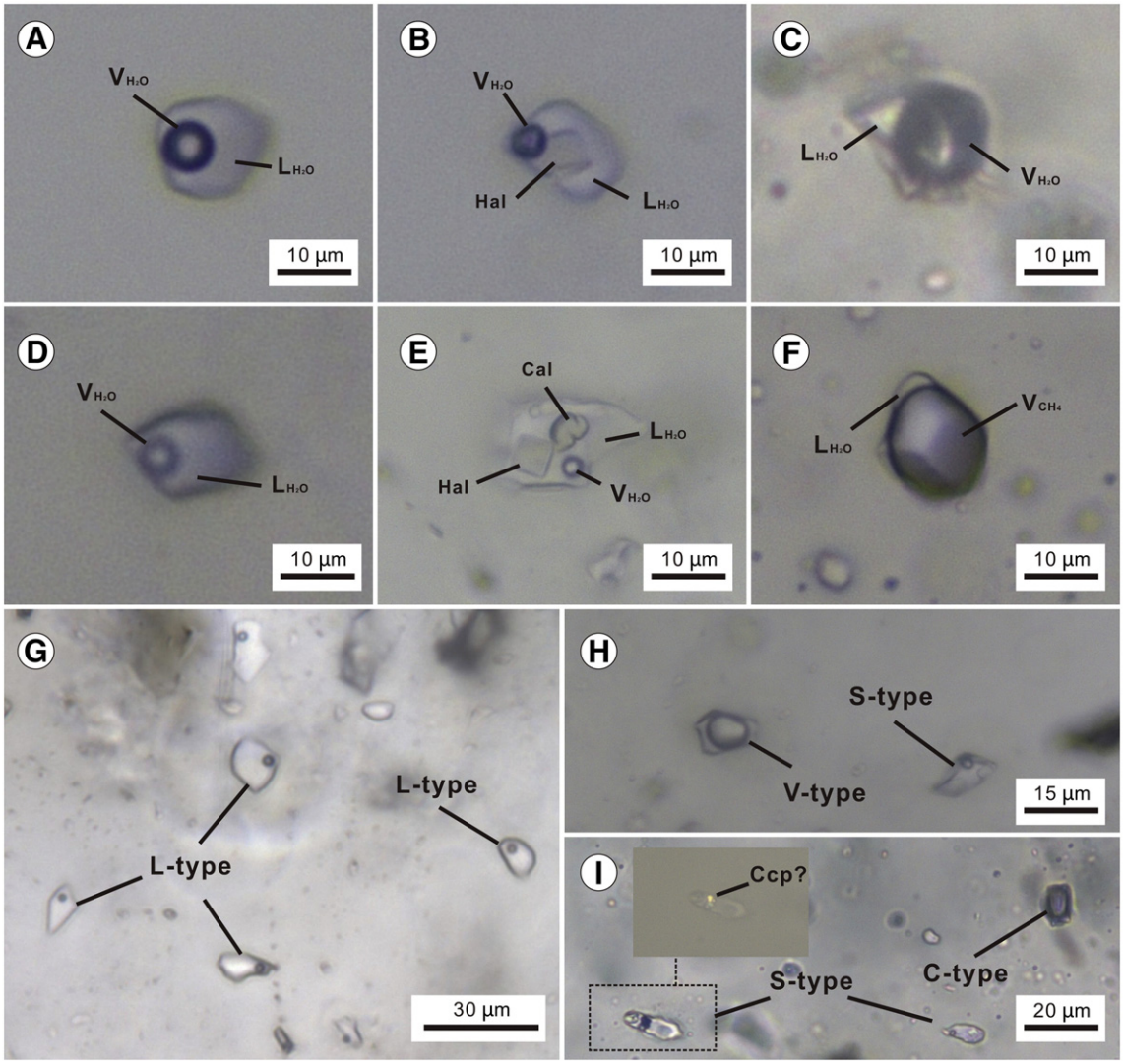

Fig. 6. Photomicrographs of the Luojiahe fluid inclusions (FIs). (A). Stage I L-type FI with V_{H2O} and L_{H2O}. (B). Stage I S-type FI with a halite daughter mineral. (C). Stage I V-type FI with V_{H2O} and L_{H2O}. (D). Stage II L-type FI with V_{H2O} and L_{H2O}. (E). Stage II S-type FI with halite and calcite daughter minerals. (F). Stage II C-type FI with Vc_{H4} and L_{H2O}. (G). Randomly distributed Stage I L-type FIs in Q1. (H). Stage I V- and S-type FIs coexist in Q2. (I). Stage II C- and S-type FIs coexist in Q3. The upper left photo taken under reflected light. Abbreviations: Vc_{H4} = CH_4 vapor; V_{H2O} = H_2O vapor; L_{H2O} = H_2O liquid; Hal = halite; Cal = calcite; Ccp = chalcopyrite.

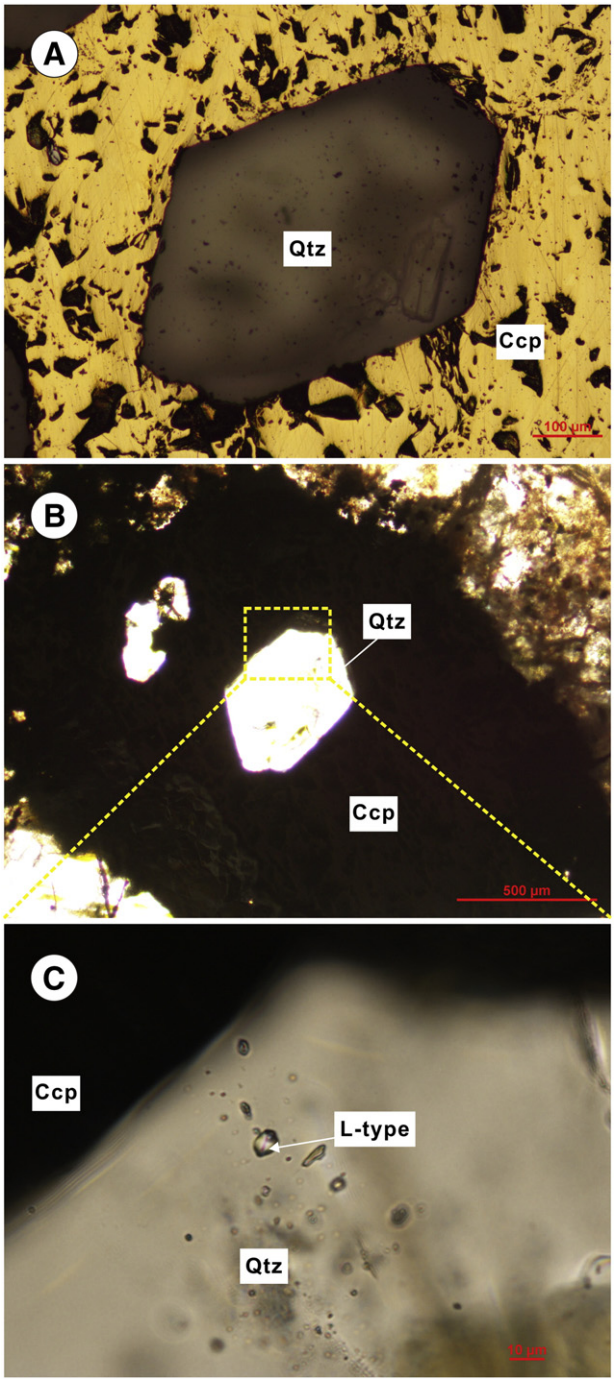

Fig. 7. Photomicrographs of the Stage I unstrained quartz grains (Q1) and their FIs. (A) and (B). Q1 in chalcopyrite with straight grain boundary. (C). L-type FIs in Q1. Abbreviations: Qtz = dolomite; Ccp = chalcopyrite.

et al., 1990; Chi and Ni, 2007). Ice melting temperatures of the L-type FIs vary from −37.5 to −23.6 °C, with corresponding salinities of 23.9–27.9 wt.% NaCl equiv. (Fig. 8A and B). The total homogenization to liquid occurred at 125 to 220 °C. In contrast, the L-type FIs of Q3 (Stage II) have eutectic temperatures varying from −21.2 to −20.8 °C, representing a NaCl-H_2O system. The different systems between the L-type FIs in Q1 and Q3 indicate that they were derived from different fluid sources. The L-type FIs in Q3 have ice melting temperatures of −12.1 to −7.1 °C, and salinities of 10.6–15.9 wt.% NaCl equiv. (Fig. 8C and D). The L-type FIs in Q3 have higher homogenization temperatures (192–305 °C) than their Q1 counterparts.

2) V-type FIs: The V-type inclusions in Q2 have eutectic temperatures of −21.2 to −20.6 °C, ice melting temperatures of −4.3 to −1.2 °C, and salinities of 2.1 to 6.9 wt.% NaCl equiv. Their homogenization temperatures vary from 265 to 363 °C. Only a few successful runs were obtained, and most of the V-type FIs with high vapor/liquid ratios decrepitated during heating.
3) S-type FIs: S-type inclusions in Q2 usually homogenized by halite disappearance (rarely by vapor bubble disappearance) at 249–339 °C, with corresponding salinities of 34.5–42.2 wt.% NaCl equiv. (Fig. 8A and B). All the S-type FIs in Q3 homogenized by halite disappearance at 225–350 °C, with corresponding salinities of 34–43.2 wt.% NaCl equiv. (Fig. 8C and D).
4) C-type FIs: When cooled below −100 °C, C-type FIs in Q3 nucleated a vapor bubble and all phases were frozen at −182.5 to −182.9 °C. These FIs partially homogenize to liquid at −89.5 to −95.8 °C (Fig. 9). Given that the critical point temperature of CH_4 is −82.6 °C, the fluid composition is predominated by CH_4 (Buruss, 1981; Ramboz et al., 1985; Fan et al., 2000). Minor gases of other types may be present, but they were not detected in the laser Raman spectroscopy analysis (Fig. 11B). The C-type FIs with large bubble volumes decrepitated at 261–355 °C, and thus their homogenization temperatures could not be obtained.

5.3. Laser Raman spectroscopy analysis

Laser Raman spectroscopy analysis shows that the vapor phase compositions of C-type FIs are primarily CH_4 (2914 cm^{-1}; Fig. 11B), consistent with the microthermometric results (Fig. 9). H_2O is the dominant vapor phase composition for all V-, S- and L-type FIs (Fig. 11A and D). Calcite (1083 cm^{-1}; Fig. 11C) daughter mineral was identified in the S-type FIs from Q3.

5.4. Carbon and oxygen isotopes

Carbon and oxygen isotopic data of this study and compiled from Zhen et al. (1993) were presented in Table 3 and Fig. 12. The Stage II calcite shows an elongated data distribution in the C-O isotope diagram (Fig. 12). The $\delta^{18}O_{V\text{-}SMOW}$ values exhibit a relatively narrow range (10.75 to 12.20‰), indicating a relatively uniform oxygen isotopic composition, whereas the $\delta^{13}C_{V\text{-}PDB}$ values exhibit a considerably wider range (−4.58 to −10.83‰). Most of the data points fall within the

Table 2
Microthermometric data of fluid inclusions in the Luojiahe Cu deposit.

Stage	Quartz type	Inclusion type	Number	Tm,CH_4 (°C)	ThCH_4 (°C)	Ti (°C)	Tm,ice (°C)	Th (°C)	Salinity (wt.% NaCl)
I Stage	Q1	L	62			−62.4 to −51	−37.5 to −23.6	125–220	23.9–27.9
	Q2	V	11			−21.2 to −20.6	−4.3 to −1.2	265–363	2.1–6.9
	Q2	S	56					249–339	34.5–42.2
II Stage	Q3	S	74					225–350	34–43.2
	Q3	C	36	−182.5 to −182.9	−89.5 to −95.8				
	Q3	L	26			−21.2 to −20.8	−12.1 to −7.1	192–305	10.6–15.9

Tm,CH_4 (°C): melting temperature of CH_4; ThCH_4 (°C): partial homogenization temperature of CH_4; Ti (°C): first ice-melting temperature; Tm,ice (°C): temperature of ice point; Th (°C): final homogenization temperature.

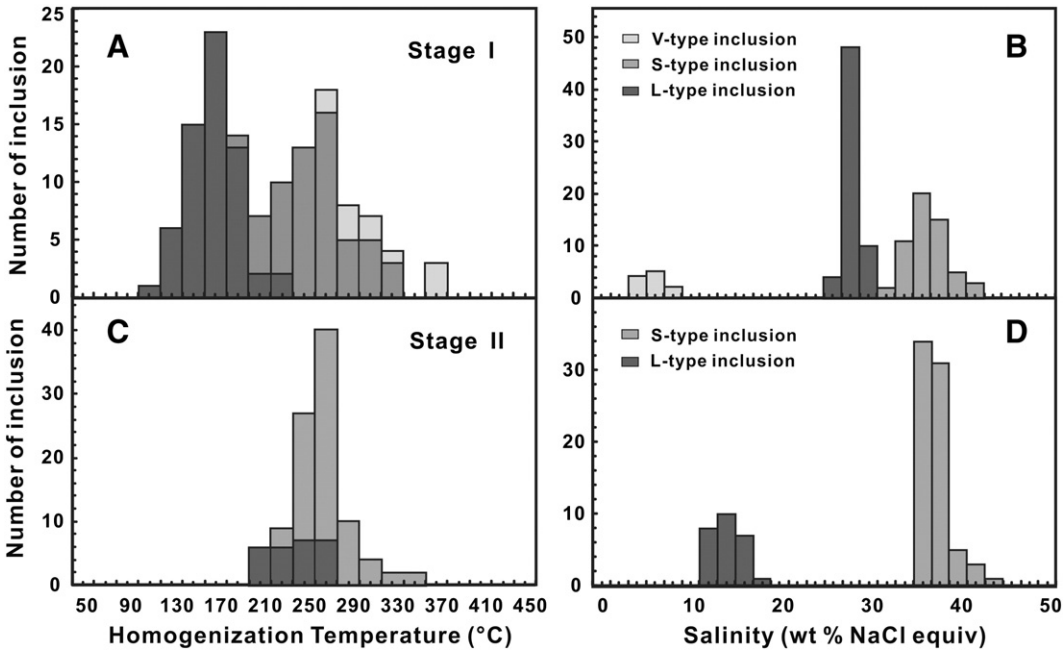

Fig. 8. Histograms of salinities and homogenization temperatures for the Stages I and II FIs.

field of the Besshi mafic volcanogenic hydrothermal carbonate (Biondi et al., 2013).

Organic carbon isotopic analysis for graphite shows that the $\delta^{13}C_{V\text{-}PDB}$ values vary from −32.01 to −39.16‰. Organic carbon isotopic data of this study and those in the previous literatures are presented in Fig. 13.

5.5. Hydrogen and oxygen isotopes

Hydrogen and oxygen isotopic compositions of four Q2 and Q3 quartz samples were listed in Table 4. The $\delta^{18}O_{H2O}$ were calculated using the equation $1000\ln\alpha_{quartz\text{-}H2O} = 3.38 \times 10^6\ T^{-2} - 3.40$ (Clayton et al., 1972). The average temperatures of the Q2 and Q3 FIs are 279 °C and 307 °C, respectively. The $\delta^{18}O$ of quartz is of 11 to 11.7‰, corresponding to $\delta^{18}O_{H2O}$ of 3.3 to 5.0‰. The δD_{H2O} varies from −42 to −64.7‰.

6. Discussion

6.1. Primary fluid compositions and characteristics of VMS mineralization

6.1.1. Preservation of primary fluid inclusions

The preservation of primary FIs in metamorphosed VMS deposits is highly controversial (Ripley and Ohmoto, 1977; Broman, 1987; Hall, 1989; Giles and Marshall, 1994; de Ronde et al., 1997; Lowe and Byerly, 2003; Moura, 2005; Bradshaw et al., 2008; Xu et al., 2011). Ripley and Ohmoto (1977) first reported that primary FIs in the Raul VMS Cu deposit (Peru) underwent amphibolite-facies metamorphism. Many subsequent studies also supported that primary FIs in metamorphosed VMS deposits could be preserved, e.g., at the Skellefete metallogenic province (northern Sweden) (Broman, 1987), Barberton greenstone belt (South Africa) (de Ronde et al., 1997), and the Gacun VMS deposit (China) (Hou et al., 2001), yet such conclusion was also disputed by many others (Hall, 1989; Giles and Marshall, 1994;

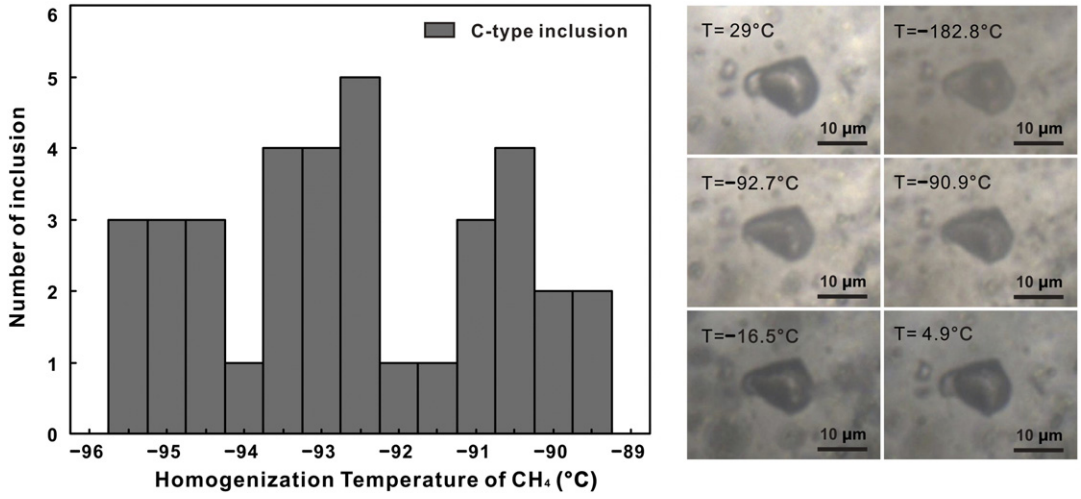

Fig. 9. Histogram of the partial homogenization temperatures of C-type FIs. Photomicrographs show the microthermometric process of a representative C-type FI in Q3. The C-type FI nucleated a vapor bubble and all phases were frozen at −182.8 °C. It homogenized partially to liquid at −90.9 °C.

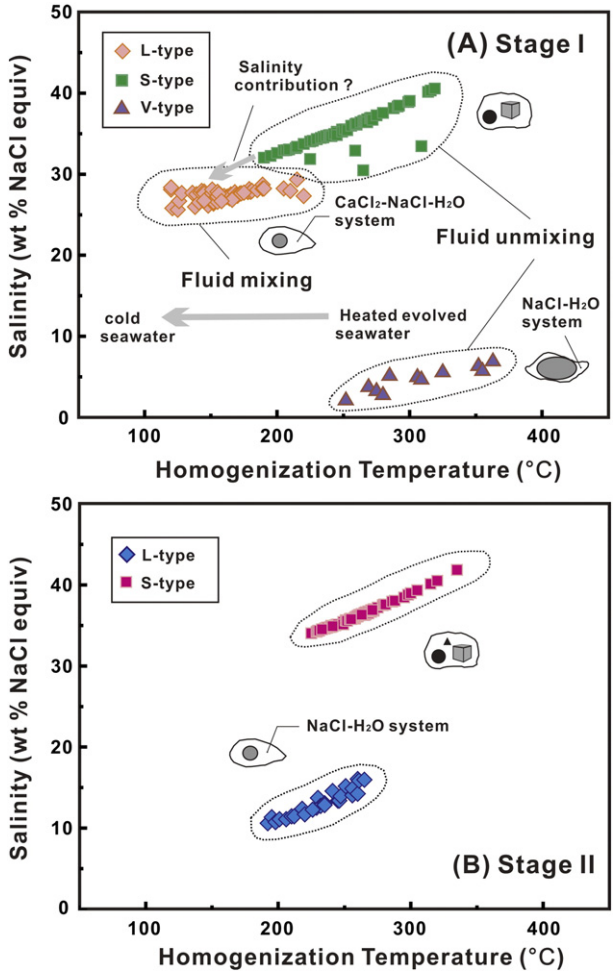

Fig. 10. Homogenization temperatures vs. salinities diagram for the Stages I and II FIs. (A). S- and V-type FIs in Q2 have similar homogenization temperatures, showing fluid unmixing features. Their salinities have a relatively narrow range despite the decrease of the homogenization temperatures, suggesting a mixing between hot evolved seawater and cold seawater. (B). Homogenization temperatures vs. salinities diagram for the Stage II S- and L-type FIs.

Marshall et al., 2000), which argued that all the FIs in metamorphosed VMS deposits should have been (post)-metamorphic (Marshall et al., 2000).

Moura (2005) recently reported the presence of both primary exhalative fluids (in massive sulfide ores) and metamorphogenic fluids (in stockwork ores) at the Neves Corvo VMS deposits (Iberian Pyrite Belt). Our study on the Luojiahe FIs also shows that the quartz grains (Q1) in the banded ore sulfides can also preserve primary FIs (Fig. 7C). Actually, as most of the quartz grains in the banded ores were recrystallized during subsequent deformation and metamorphism, the majority of primary inclusions have been eliminated. However, Q1 remained unstrained because the ductile nature of the hosting-sulfides can take up the strain during metamorphism (Fig. 7A and B). Thus, Q1 can preserve the primary fluid inclusions.

6.1.2. High salinity evolved seawater

6.1.2.1. H_2O-NaCl-$CaCl_2$ fluid system. Recent crushing/leaching analyses of VMS fluid composition confirmed the presence of Ca^{2+} (Graupner et al., 2001). Geochemical experiments also showed that seawater-basalt interaction could produce Cu-rich Na-Ca-Cl solution (Bischoff and Dickson, 1975), thus it is well accepted that the VMS fluids consist of a H_2O-NaCl-$CaCl_2$ system (Steele-MacInnis et al., 2011; Bodnar et al., 2014).

The eutectic temperatures (ca. −52 °C) of the L-type FIs in Q1 demonstrated that the ore-forming fluid system was a H_2O-NaCl-$CaCl_2$ system. In fact, it was associated with the spilite located in the bottom of the orebodies (Fig. 3). Given that spilite was supposed to be altered and weakly metamorphosed basalt, they played an important role in the mass balance of Ca and Na in the rocks and hydrothermal systems (Staudigel, 2014). Thus, the H_2O-NaCl-$CaCl_2$ fluid system of the L-type FIs in Q1 could represent the evolved seawater that reacted with original basalt at Stage I.

6.1.2.2. High salinity and low temperature fluid system. As shown in the Figs. 8B and 10A, the Stage I L-type FIs have significantly higher salinity (23.9–27.9 wt.% NaCl equiv.) than typical VMS deposits (3.0–10 wt.% NaCl equiv.; Hou et al., 2008). This may have been led by:

1) The long-lived cratonic bodies are absent in the Archean, which may have prevented the evaporite deposition and thus the brine preservation in sedimentary basins (Knauth, 2005). As a consequence, Archean seawater was almost three times more saline than modern seawater (Knauth, 2005; Huston et al., 2010). Available FI data also indicate that the ore-forming fluids of some Archean and Proterozoic VMS deposits have salinity of 6–24 wt.% NaCl equiv. (Huston et al., 2010).
2) Magmatic-hydrothermal activities may further increase the fluid salinity (e.g., Millenbach, 27–47 wt.% NaCl equiv.: Lao, 1982; Mattagami Lake, 20–35 wt.% NaCl equiv.: Costa et al., 1983; see Section 6.1.3; Fig. 10A).

The L-type FIs in Q1 have relatively low homogenization temperature (125 to 220 °C), consistent with typical VMS deposits (100–360 °C) (Bodnar et al., 2014). Their salinities have a relatively narrow range despite the decrease of the homogenization temperatures (Fig. 10A), which may represent a mixing between the hot evolved seawater and cold seawater in the near-surface environment (Fig. 10A; Franklin et al., 2005; Hou et al., 2008). The mixing can change the temperature and pH of the ore-forming fluids, leading to the Stage I metal precipitation.

6.1.3. Magmatic fluids and fluid unmixing

The VMS hydrothermal fluid system comprises a variable mix of evolved seawater (dominant) and magmatic fluids (Franklin et al., 1981; Huston et al., 2010). In some cases, magmatic degassing releases high temperature, saline and metal-rich fluids into the seafloor hydrothermal systems, and play an important role in the VMS metallogeny (e.g., Costa et al., 1983; Yang and Scott, 1996; Shanks, 2001; Yang and Scott, 2005; Hou et al., 2008; Chen et al., 2015; Seewald et al., 2015).

Our study shows that the compositions (H_2O-NaCl system) and FI assemblages (S-type and V-type FIs) of Q2 are totally different from Q1 (H_2O-NaCl-$CaCl_2$ system and L-type FIs). Different from the evolved seawater represented by FIs in Q1, the FIs in Q2 may signify the participation of magmatic fluids in the Stage I mineralization, as evidenced by:

1) High temperature (249–339 °C; Fig. 8A) and salinity (34.5–42.2 wt.% NaCl equiv.; Fig. 8B) of the S-type FIs in Q2 are consistent with a magmatic origin (Yang and Scott, 1996; Franklin et al., 2005; Hou et al., 2008).
2) The sample from Q2 has hydrogen and oxygen isotopic compositions extremely close to the magmatic water box (Fig. 14), suggesting that the fluids were possibly predominantly magmatic.
3) The S-type and V-type FIs in Q2 have highly similar homogenization temperature ranges, but are very different in terms of their salinity ranges and ways of homogenization (Fig. 10A). The coexistence of the two Q2 FI types suggests that the fluid system may have experienced local unmixing (Fig. 6H), which may have been caused by the pressure fluctuation during the upward migration of magmatic fluids along syn-volcanic fractures (Vanko, 1988; Zaw et al., 1994;

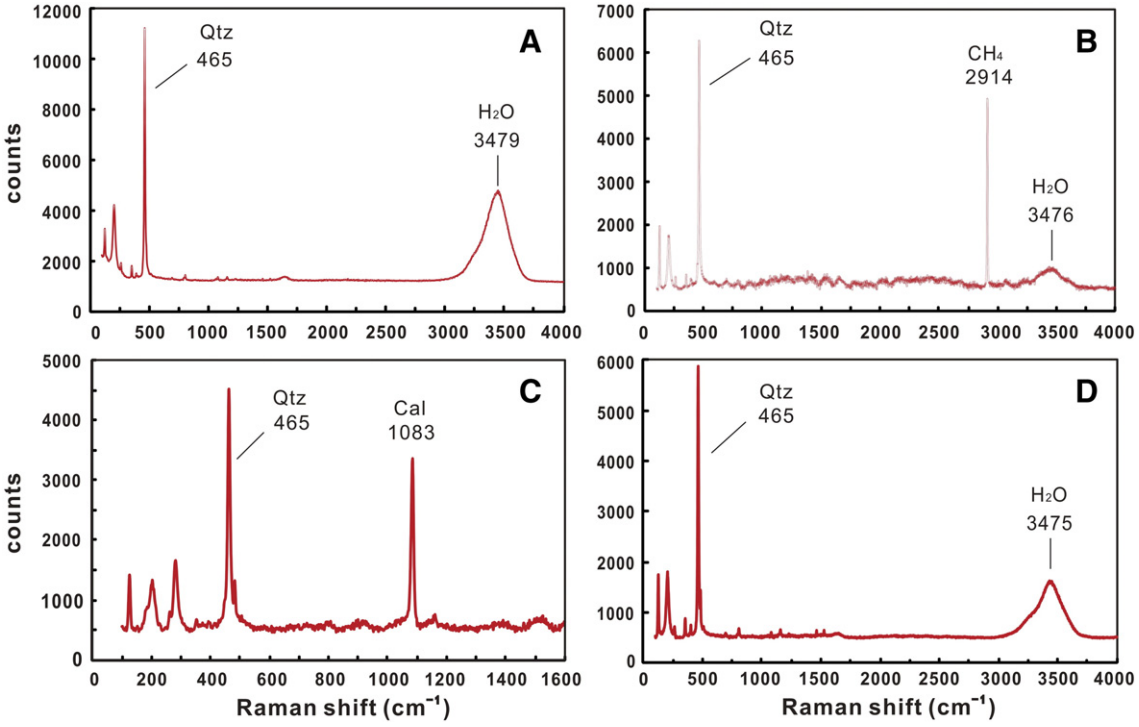

Fig. 11. The laser Raman spectra of FIs. (A). H_2O-spectra of the vapor in a L-type FI from Q1. (B). CH_4-spectra of the vapor in a C-type FI from Q3. (C). Calcite-spectra of the daughter mineral in a S-type FI from Q3. (D). H_2O-spectra of the vapor in a V-type FI from Q2.

Moura, 2005), leading to the stockwork ore formation (Hou et al., 2008).

As mentioned in Section 6.1.2.2, ascending of the high salinity magmatic fluids may contribute to the elevated salinity of the shallow evolved seawater (Fig. 10A).

6.2. Sources of CH_4-rich fluids and their role in Stage II mineralization

6.2.1. Sources of CH_4-rich fluids

The widespread CH_4-rich FIs (C-type) in Q3 indicate that CH_4 may have been important in the Stage II Cu mineralization. CH_4-rich FIs were widely reported in different ore deposit types, e.g., Archean greenstone-hosted Au deposits (Naden and Shepherd, 1989; Fan et al., 2000; Polito et al., 2001), reduced porphyry Cu deposits (Shen et al., 2010; Cao et al., 2014a, 2014b), sediment-hosted stratiform Cu deposits (McGowan et al., 2003), and epithermal Au-Ag deposits (Albinson et al., 2001). Although CH_4 was detected in both fossilized VMS systems and modern submarine hydrothermal vents (Lilley et al., 1993; Hou et al., 2008), the reports about FIs containing CH_4 as a discrete and significant phase in VMS systems are still rare.

In general, CO_2 is the dominant volatile component of ore-forming fluids in metamorphosed VMS deposits (Inverno and Solomon, 2001; Chen et al., 2007; Bradshaw et al., 2008; Xu et al., 2011), whose generation was interpreted to be caused by metamorphic devolatilization of the host rocks (Cartwright and Oliver, 2000). So why the significant volatile of metamorphic ore-forming fluids in the Luojiahe deposit is CH_4

Table 3
Carbon and oxygen isotopes from the Luojiahe copper deposit. $\delta^{18}O_{V\text{-}SMOW(‰)} = 1.03091 \times \delta^{18}O_{V\text{-}PDB(‰)} + 30.91$, according to Coplen et al. (1983).

Sample	$\delta^{18}O_{VPDB}$	$\delta^{13}C_{VPDB}$	$\delta^{18}O_{V\text{-}SMOW}$	Reference
Mineralized calcite of the II stage				
14LJK6-1	−18.66	−4.58	11.67	This study
LJH6-1	−18.32	−6.03	12.02	This study
LJH4-7	−18.15	−6.66	12.20	This study
13LJH1-1	−19.55	−10.83	10.75	This study
L600-1	−17.32	−5.92	12.66	Zhen et al. (1993)
Barren ore-bearing calcite in spilite				
LY-72	−17.74	−1.36	12.24	Zhen et al. (1993)
Barren ore-bearing calcite in chlorite schist				
LY-349	−19.07	−0.96	10.91	Zhen et al. (1993)
Graphite in chlorite schist				
13LJK2-5		−37.50		This study
LJK2-1		−32.17		This study
LJK2-1b		−32.01		This study
LJK2-4		−39.16		This study

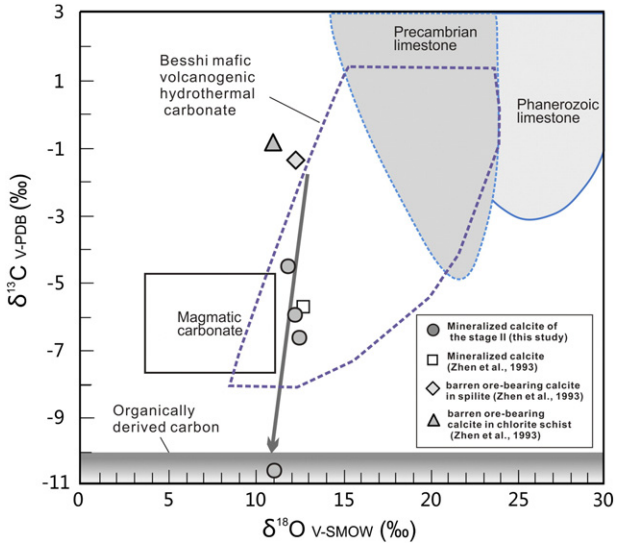

Fig. 12. Carbon- and oxygen isotopic compositions of the Luojiahe Cu deposit. Fields of magmatic carbonate and Besshi mafic volcanogenic hydrothermal carbonate are from Biondi et al. (2013); Precambrian- and Phanerozoic limestone data are from Bell and Simonetti (2010); Organic carbon data are from Longstaffe (1989).

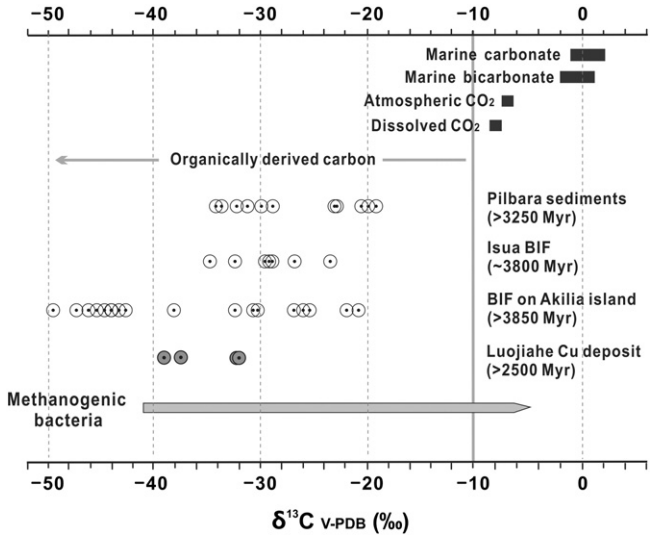

Fig. 13. Organic carbon isotopic compositions of the Luojiahe graphite. The carbon isotopic data of the Pilbara sediments, Isua BIF and BIF on Akilia island are from Mojzsis et al. (1996). The data of marine carbonate, marine bicarbonite, atmospheric CO_2, dissolved CO_2, and methanogenic bacteria are from Schidlowski (2001). Field of organic carbon is from Longstaffe (1989).

rather than CO_2? More importantly, as the ore-hosting chlorite schist contains abundant graphite, the equilibria between devolatilization-released H_2O and graphite may have controlled the oxygen fugacity (fO_2) of the graphite-rich strata (French, 1966; Frost, 1979). Furthermore, the compositions of metamorphic C-H-O fluids are sensitive to temperature- and fO_2 changes (Holloway, 1981; Crawford and Hollister, 1986). Thus, the presence of graphite in the wall rocks may have significantly influenced the metamorphic fluid compositions. Based on experimental evidence and geological conditions, Holloway (1984) pointed out that at below 300 °C (or up to 400 °C in highly saline systems), metamorphism of graphite-bearing rocks would produce CH_4-H_2O rather than CO_2-H_2O fluids. Based on our Luojiahe FI and stable isotopic data, we propose that the CH_4 was resulted from the interaction between the metamorphic ore-forming fluids and the graphite in the chlorite schist, as illustrated by the following equation (Bottrell et al., 1988):

$$C + 2H_2O = CH_4 + 2[O]. \quad (1)$$

[O] in reaction (1) denotes chemically bound oxygen rather than free O_2 in the fluid phase. This oxygen can be partly balanced by the reaction with graphite to produce CO_2, but the temperature conditions and the presence of graphite would constrain the CO_2 development in the fluids (Holloway, 1984). Regarding the absence of CO_2, the presence of calcite in S-type FIs and in the mineralized veins/altered wall-rocks at Luojiahe (Figs. 5D and 6E), the liberated CO_2 and [O] may be confined in calcite by reacting with Ca in the metamorphic ore-forming fluids (Bottrell et al., 1988):

$$Ca_{(aq)} + CO_2 + [O] = CaCO_3. \quad (2)$$

Table 4
Hydrogen and oxygen isotopes for quartz from the Luojiahe copper deposit. $\delta^{18}OH_2O$ (‰) values are calculated according to Clayton et al. (1972).

Sample	Vein type	Th (°C)	$\delta^{18}O_{quartz}$	$\delta^{18}O_{H2O}$	$\delta^{18}D_{H2O}$
LJK1-9	Q2	307	11.7	5.1	−51.7
14LJK6-3	Q3	279	11.3	3.6	−44.8
13LJH5-2	Q3	279	11.0	3.3	−64.7
LJA1-1	Q3	279	11.2	3.5	−42.0

Abbreviation: Th: average homogenization temperature of every vein type.

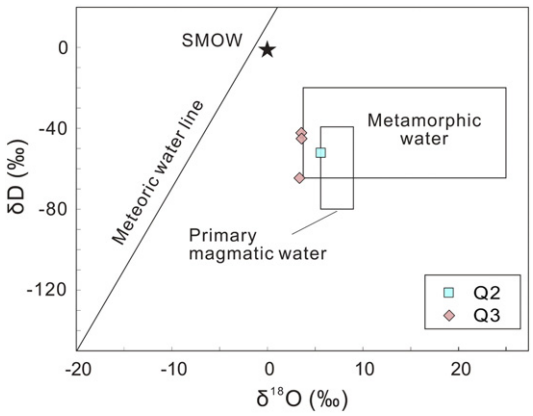

Fig. 14. Hydrogen- and oxygen isotopic compositions of the Luojiahe Cu deposit. Fields of primary magmatic waters and metamorphic waters are from Taylor (1974).

We thus propose that the CH_4 enrichment was due to the reactions with the graphite (Fig. 15), as evidenced by:

1) The microthermometric results show that the S- and L-type FIs in Q3 have homogenization temperatures of 192 to 350 °C, with corresponding salinities of 10.6–43.2 wt.% NaCl equiv. (Figs. 8C, D, and 10B). The temperatures are comparable with greenschist-facies metamorphism at Luojiahe (Zhen et al., 1993). These temperatures and salinities are also consistent with the formation of the CH_4-H_2O system (below 400 °C; salt-rich systems) (Holloway, 1984) mentioned earlier.
2) Hydrogen and oxygen isotopic results show that the Q3 fluids were likely to be metamorphic (Fig. 14). Metamorphic water can be produced by metamorphic devolatilization of mafic-ultramafic rocks, which have reacted with low-medium temperature hydrothermal fluids following their formation (Cartwright and Oliver, 2000). Thus, as one of the two reactants in the reaction (1), H_2O may have been derived from metamorphic devolatilization of the Luojiahe spilite and chlorite schist.
3) The Stage II calcite has a considerably wide range of carbon isotopic compositions (−4.58 to −10.83‰), with the lowest value (−10.83‰) probably reflecting an organic carbon source (Fig. 12). Given that the carbon isotopic fractionation between minerals and fluids does not depend significantly on temperature (O'Neil et al., 1969), the C-O isotopic trend in Fig. 12 may have been led by the mixing of different carbon isotope sources. By contrast, the $\delta^{13}C_{V\text{-}PDB}$ of graphite in the Luojiahe chlorite schist is of −32.01 to −39.16‰ (Table 3), indicating clearly an organic origin (Fig. 13). Thus, we propose that the metamorphic ore-forming fluids may have exchanged carbon isotopes with the graphite.

6.2.2. Metallogenic role of CH_4-rich fluids at Stage II

With reaction (1) proceeding, the ore-forming fluids at Luojiahe may have been reduced by graphite, and the fluid system's fO_2 buffered by reaction (1). Thus, the equilibration between the metamorphic ore-forming fluids and graphite is crucial to the Stage II mineralization. As CH_4 was released into the fluid phase, the CH_4-NaCl-H_2O fluid system was formed. However, this system was unstable because the presence of NaCl would significantly increase the range of CH_4-H_2O immiscibility by expanding the compositional range of fluid unmixing and raising the temperature of the consolute point (Takenouchi and Kennedy, 1964; Naumov et al., 1974; Gehrig et al., 1979; Crawford and Hollister, 1986). Accompanied by the H_2O consumption in the ore-forming fluids by reaction (1), the fluids would become even more saline. Finally, CH_4 saturation in the fluid system would result in the occurrence of two immiscible fluid phases: CH_4-rich fluid and NaCl brine. This can explain the coexistence of C- and S-type FIs in Q3 (Fig. 6I). In addition, the CH_4

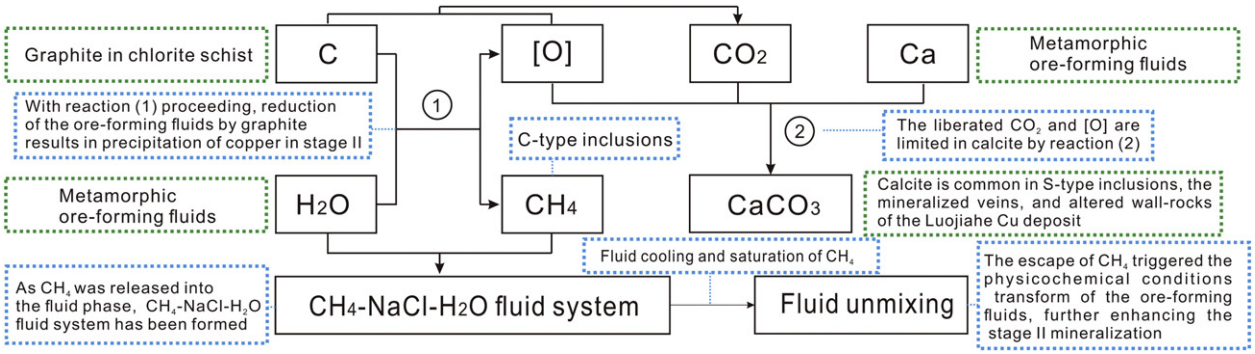

Fig. 15. Model of the redox reactions and fluid mineralization mechanism at Stage II.

escape may have triggered changes in the physicochemical conditions of the ore-forming fluids, further promoting the Stage II mineralization.

6.3. Origins of graphite and microbial generation in VMS systems

As aforementioned, the occurrence of abundant graphite in the Luojiahe chlorite schist is critical to the Stage II mineralization, and thus the origin of graphite is worthy to explore. In many Archean sedimentary strata, biogenic graphite has commonly $\delta^{13}C_{V\text{-}PDB}$ of below −19‰ (Fig. 13). Carbon isotopic analysis shows that the $\delta^{13}C_{V\text{-}PDB}$ values of our graphite samples fall in the range of −40 to −10‰, largely indicative of biogenic carbon sources (Mojzsis et al., 1996; Rosing, 1999; Schidlowski, 2001). The Luojiahe carbon isotopic data also fall in the Akilia island BIF field (Fig. 13), which was interpreted to represent the possible earliest life on Earth (Mojzsis et al., 1996).

Nevertheless, the conclusion on graphite derived from organic matter is ambiguous only on the basis of carbon isotopic values (Schidlowski, 2001; Brasier et al., 2002; van Zuilen et al., 2003; Bernard and Papineau, 2014). We propose that graphite in the Luojiahe copper deposit was derived from original sedimentary organic matter in seafloor hydrothermal vent systems. The evidence is as follows:

1) The Archean VMS systems were favorable for the thriving of microbial communities, as demonstrated by the abundant microfossils (thermophilic chemotropic prokaryotes) in the Paleoarchean (ca. 3235 Ma) VMS deposit in the Pilbara Craton (West Australia) (Rasmussen, 2000). McCollom (2000) suggested that the biomass generated in seafloor hydrothermal systems is ca. 1000 times more than normal seafloor environment, due mainly to the near-continuous supply of nutrients and metals essential for microbial growth by the hydrothermal fluids (Seyfried et al., 2015; Westall et al., 2015). Furthermore, the Fe-rich basaltic (e.g., with Fe-rich spilite) environment in the Archean ocean also promoted the development of sulfate-reducing microbes (Crowe et al., 2014; Ueno, 2014). For the Luojiahe case, such biomass accumulated during the VMS mineralization may have transformed into graphite in the subsequent metamorphism.
2) The calculations by Katsev and Crowe (2015) suggest that the buried fraction of deposited organic carbon may have been 6–40 times higher in Precambrian anoxic oceans than today. The Precambrian anoxic oceans preserved organic carbon better, as also supported by the common existence of graphite in many Archean greenstone belts (Springer, 1985).
3) Thermodynamic equilibria show that the graphite $^{13}C/^{12}C$ increases with increasing metamorphic grade (Schidlowski, 2001), and metamorphic overprinting always pushes up $\delta^{13}C_{V\text{-}PDB}$ to more positive values (Buseck and Beyssac, 2014). The lowermost $\delta^{13}C_{V\text{-}PDB}$ values of graphite are consequently the least exchanged and most original (Schidlowski, 2001). Therefore, the relatively low $\delta^{13}C_{V\text{-}PDB}$ (−32.01 to −39.16‰) of the Luojiahe graphite was unlikely to be resulted from metamorphic overprint.

6.4. Mechanism of fluid mineralization

A series of Neoarchean greenstone-hosted VMS Cu deposits were recently discovered in the Wutai Greenstone Belt (Trans-North China Orogen) (Li et al., 2004; Polat et al., 2005; Niu et al., 2009). The Wutai VMS deposits were spatially associated with mafic volcanic-sedimentary sequences and were modified by subsequent metamorphism (Li et al., 2004). The ore-forming environment, mineralization characteristics and formation ages of the Wutai VMS Cu deposits are comparable with the Luojiahe Cu deposit in the ZTS. The Luojiahe copper deposit also experienced two mineralization stages, including primary VMS mineralization (Stage I) and metamorphic remobilization (Stage II). Here, we propose a new model of the hydrothermal fluid evolution and mineralization for the Luojiahe Cu deposit.

At Stage I, the heating of the underlying syn-volcanic magmas induced the interaction between the modified seawater and the upper basalt, producing a Cu-rich H_2O-NaCl-$CaCl_2$ hydrothermal fluid system. With the heated Cu-bearing fluids migrating upwards along syn-volcanic faults onto the seafloor or into the shallow and permeable volcaniclastic rocks, fluid mixing between the hot evolved seawater and cold seawater may have occurred. This may have changed the temperature and pH of the ore-forming fluids and precipitated the metals. Organic activities in near-surface environment may have participated to fix chalcophile elements into the sulfides (Franklin et al., 2005). In addition, high temperature and salinity fluids may have yielded during the fluid unmixing, caused possibly by the pressure fluctuation during the magmatic fluid percolation along fractures. The original magmatic fluids may have separated into a low density vapor phase and a high salinity liquid phase, resulting in the formation of stockwork ores.

At Stage II, the primary VMS ores were remobilized by metamorphism during the Zhongtiao Movement. Massive metamorphic water may have been produced by metamorphic devolatilization of the ore-hosting spilite and chlorite schist. With the metamorphic ore-forming fluids migrating into graphite-rich chlorite schist, the graphite-H_2O interaction may have reduced the ore-forming fluids, released CH_4 into the fluid phase and precipitated Cu (Fig. 15). With the consumption of H_2O in the hydrothermal fluid system, the consequent salinity increase may have led to CH_4 saturation in the CH_4-NaCl-H_2O fluid system (Fig. 15), and the subsequent fluid unmixing may further promote the Stage II mineralization.

7. Conclusions

1. The Luojiahe Cu deposit underwent two mineralization stages, i.e., primary VMS mineralization (Stage I) and metamorphic remobilization (Stage II). The Stage I ore-forming fluids consist predominantly

of evolved seawater (125–220 °C; 23.9–27.9 wt.% NaCl equiv.) and minor magmatic fluids (249–339 °C; 34.5–42.2 wt.% NaCl equiv.).
2. The main Stage I mineralization may have led by 1) fluid mixing of heated evolved seawater and cold seawater in the near-surface environment; and 2) fluid unmixing led by magmatic fluids percolating into syn-volcanic faults, forming the stockwork ores.
3. The Stage II ore-forming fluids comprise CH_4-rich metamorphic fluids (192–350 °C; 10.6–43.2 wt.% NaCl equiv.).
4. The graphite-H_2O interaction may have generated CH_4, reduced the ore-forming fluids and precipitated Cu (Stage II). The consequent H_2O consumption in the hydrothermal fluid system increased the fluid salinity and may have triggered the fluid unmixing in the CH_4-NaCl-H_2O system, further enhancing the Stage II Cu mineralization.
5. Graphite in the Luojiahe Cu deposit may have been derived from sedimentary organic matter formed in the seafloor hydrothermal vent system.

Acknowledgements

This study was financially supported by the National Basic Research Program of China (no. 2012CB416603). The Zhongtiaoshan Non-Ferrous Metals Group Co., Ltd. is thanked for its field assistance. We thank Drs. Bo Wei and Rongqing Zhang (Guangzhou Institute of Geochemistry, CAS) for their constructive suggestions. Cenozoic Geoscience Editing & Consultancy is thanked for the language editing. This is contribution No. IS-2263 from GIGCAS.

References

Albinson, T., Norman, D., Cole, D., Chomiak, B., 2001. Controls on formation of low-sulfidation epithermal deposits in Mexico: constraints from fluid inclusion and stable isotope data. Special Publication-Society of Economic Geologists. 8, pp. 1–32.
Bai, J., 1997. Precambrian crustal evolution of the Zhongtiao Mountains. Earth Sci. Front. 4, 281–289 (in Chinese with English abstract).
Bell, K., Simonetti, A., 2010. Source of parental melts to carbonatites–critical isotopic constraints. Mineral. Petrol. 98, 77–89.
Bernard, S., Papineau, D., 2014. Graphitic carbons and biosignatures. Elements 10, 435–440.
Biondi, J.C., Santos, R.V., Cury, L.F., 2013. The Paleoproterozoic Aripuanã Zn-Pb-Ag (Au, Cu) volcanogenic massive sulfide deposit, Mato Grosso, Brazil: geology, geochemistry of alteration, carbon and oxygen isotope modeling, and implications for genesis. Econ. Geol. 108, 781–811.
Bischoff, J.L., Dickson, F.W., 1975. Seawater-basalt interaction at 200 °C and 500 bars: implications for origin of sea-floor heavy-metal deposits and regulation of seawater chemistry. Earth Planet. Sci. Lett. 25, 385–397.
Bodnar, R., Lecumberi-Sanches, P., Moncada, D., Steele-MacInnis, M., 2014. Fluid inclusions in hydrothermal ore deposits. Treatise on Geochemistry, second ed., pp. 119–142.
Bottrell, S., Shepherd, T., Yardley, B., Dubessy, J., 1988. A fluid inclusion model for the genesis of the ores of the Dolgellau Gold Belt, North Wales. J. Geol. Soc. 145, 139–145.
Bradshaw, G.D., Rowins, S.M., Peter, J.M., Taylor, B.E., 2008. Genesis of the Wolverine volcanic sediment-hosted massive sulfide deposit, Finlayson Lake District, Yukon, Canada: mineralogical, mineral chemical, fluid inclusion, and sulfur isotope evidence. Econ. Geol. 103, 35–60.
Brasier, M.D., Green, O.R., Jephcoat, A.P., Kleppe, A.K., Van Kranendonk, M.J., Lindsay, J.F., et al., 2002. Questioning the evidence for Earth's oldest fossils. Nature 416, 76–81.
Broman, C., 1987. Fluid inclusions of the massive sulfide deposits in the Skellefte district, Sweden. Chem. Geol. 61, 161–168.
Buruss, R., 1981. Analysis of phase equilibria in COHS fluid inclusions: mineralogy. Assoc Canada Short Course Handbook. 6, pp. 39–74.
Buseck, P.R., Beyssac, O., 2014. From organic matter to graphite: graphitization. Elements 10, 421–426.
Cao, M., Qin, K., Li, G., Evans, N.J., Jin, L., 2014a. Abiogenic Fischer–Tropsch synthesis of methane at the Baogutu reduced porphyry Cu deposit, western Junggar, NW-China. Geochim. Cosmochim. Acta 141, 179–198.
Cao, M., Qin, K., Li, G., Jin, L., Evans, N.J., Yang, X., 2014b. Baogutu: an example of reduced porphyry Cu deposit in western Junggar. Ore Geol. Rev. 56, 159–180.
Cartwright, I., Oliver, N., 2000. Metamorphic fluids and their relationship to the formation of metamorphosed and metamorphogenic ore deposits. Rev. Econ. Geol. 81–95.
Chi, G.X., Ni, P., 2007. Equations for calculation of NaCl/(NaCl + $CaCl_2$) ratios and salinities from hydrohalite-melting and ice-melting temperatures in the H_2O-NaCl-$CaCl_2$ system. Acta Petrol. Sin. 23, 33–37 (in Chinese with English abstract).
Chen, M., Campbell, I.H., Xue, Y., Tian, W., Ireland, T.R., Holden, P., et al., 2015. Multiple sulfur isotope analyses support a magmatic model for the volcanogenic massive sulfide deposits of the Teutonic Bore Volcanic Complex, Yilgarn Craton, Western Australia. Econ. Geol. 110, 1411–1423.
Chen, Y.J., Fan, H.R., Pirajno, F., Lai, Y., Su, W.C., Zhang, H., 2007. Diagnostic fluid inclusions of different types hydrothermal gold deposits. Acta Petrol. Sin. 23, 2085–2108 (in Chinese with English abstract).
Chen, Y.J., Fu, S.G., Qiang, L.Z., 1992. The tectonic environment for the formation of the Xiong'er Group and the Xiyanghe Group. Geol. Rev. 38, 325–333 (in Chinese with English abstract).
Clayton, R.N., O'Neil, J.R., Mayeda, T.K., 1972. Oxygen isotope exchange between quartz and water. J. Geophys. Res. 77, 3057–3067.
Coplen, T.B., Kendall, C., Hopple, J., 1983. Comparison of stable isotope reference samples. Nature 302, 236–238.
Corliss, J.B., Dymond, J., Gordon, L.I., Edmond, J.M., 1979. On the Galapagos Rift. Science 203, 16.
Costa, U., Barnett, R., Kerrich, R., 1983. The Mattagami Lake Mine Archean Zn-Cu sulfide deposit, Quebec; hydrothermal coprecipitation of talc and sulfides in a sea-floor brine pool; evidence from geochemistry, $^{18}O/^{16}O$, and mineral chemistry. Econ. Geol. 78, 1144–1203.
Crawford, M., Hollister, L., 1986. Metamorphic fluids: the evidence from fluid inclusions. Fluid—Rock Interactions During Metamorphism. Springer, pp. 1–35.
Crowe, S.A., Paris, G., Katsev, S., Jones, C., Kim, S.T., Zerkle, A.L., et al., 2014. Sulfate was a trace constituent of Archean seawater. Science 346, 735–739.
de Ronde, C.E., 1995. Fluid Chemistry and Isotopic Characteristics of Seafloor Hydrothermal Systems and Associated VMS Deposits: Potential for Magmatic Contributions. Magmas, Fluids and Ore Deposits. Mineralogical Association Canada Short Course, pp. 479–509.
De Ronde, C.E., deR Channer, D.M., Faure, K., Bray, C.J., Spooner, E.T., 1997. Fluid chemistry of Archean seafloor hydrothermal vents: implications for the composition of circa 3.2 Ga seawater. Geochim. Cosmochim. Acta 61, 4025–4042.
Fan, H.-R., Groves, D.I., Mikucki, E.J., McNaughton, N.J., 2000. Contrasting fluid types at the Nevoria gold deposit in the Southern Cross greenstone belt, western Australia: implications of auriferous fluids depositing ores within an Archean banded iron-formation. Econ. Geol. 95, 1527–1536.
Feng, Z.P., Wang, Z.P., 2008. The Strata Division in Songjiashan Subgroup of Jiangxian Group of Late Archean in Zhongtiaoshan Area. Shanxi Metall. 6, 20–22 (in Chinese).
Franklin, J., Lydon, J., Sangster, D., 1981. Volcanic-associated massive sulfide deposits. Econ. Geol. 75, 485–627.
Franklin, J.M., Gibson, H., Jonasson, I., Galley, A., 2005. Volcanogenic massive sulfide deposits. Economic Geology 100th Anniversary. 98, pp. 523–560.
French, B.M., 1966. Some geological implications of equilibrium between graphite and a C-H-O gas phase at high temperatures and pressures. Rev. Geophys. 4, 223–253.
Frost, B.R., 1979. Mineral equilibria involving mixed-volatiles in a C-O-H fluid phase; the stabilities of graphite and siderite. Am. J. Sci. 279, 1033–1059.
Gehrig, M., Lentz, H., Franck, E., 1979. Thermodynamic Properties of Water—Carbon Dioxide—Sodium Chloride Mixtures at High Temperatures and Pressures. High-Pressure Science and Technology, Springer, pp. 539–542.
Giles, A.D., Marshall, B., 1994. Fluid inclusion studies on a multiply deformed, metamorphosed volcanic-associated massive sulfide deposit, Joma Mine, Norway. Econ. Geol. 89, 803–819.
Graupner, T., Bray, C., Spooner, E., Herzig, P., 2001. Analysis of fluid inclusions in seafloor hydrothermal precipitates: testing and application of an integrated GC/IC technique. Chem. Geol. 177, 443–470.
Gu, L.X., Liu, X.H., Zhen, Y.Q., Wang, Y.H., 1993. Rubidium-strontium and lead isotope geology of the Luojiahe granodiorite in the Zhongtiaoshan district. J. Nanjing Univ. 29, 651–657.
Hall, D.L., 1989. Fluid Evolution During Metamorphism and Uplift of the Massive Sulfide Deposits at Ducktown, Tennessee, USA.
He, Y., Zhao, G., Sun, M., Xia, X., 2009. SHRIMP and LA-ICP-MS zircon geochronology of the Xiong'er volcanic rocks: implications for the Paleo-Mesoproterozoic evolution of the southern margin of the North China Craton. Precambrian Res. 168, 213–222.
Holloway, J., 1981. Compositions and Volumes of Supercritical Fluids in the Earth's Crust. Fluid Inclusions: Applications to Petrology. pp. 13–38 (Chapter).
Holloway, J.R., 1984. Graphite-CH_4-H_2O-CO_2 equilibria at low-grade metamorphic conditions. Geology 12, 455–458.
Hou, Z.Q., Zaw, K., Rona, P., Yinqing, L., Xiaoming, Q., Shuhe, S., et al., 2008. Geology, fluid inclusions, and oxygen isotope geochemistry of the Baiyinchang pipe-style volcanic-hosted massive sulfide Cu deposit in Gansu Province, Northwestern China. Econ. Geol. 103, 269–292.
Hou, Z.Q., Zaw, K., Xiaoming, Q., Qingtong, Y., Jinjie, Y., Mingji, X., et al., 2001. Origin of the Gacun volcanic-hosted massive sulfide deposit in Sichuan, China: fluid inclusion and oxygen isotope evidence. Econ. Geol. 96, 1491–1512.
Huang, C.K., Bai, Y., Zhu, Y.S., Wang, H.Z., Shang, X.Z., 2001. Copper Deposit of China. Geological Publishing House, Beijing, pp. 142–152 (in Chinese).
Huston, D.L., Pehrsson, S., Eglington, B.M., Zaw, K., 2010. The geology and metallogeny of volcanic-hosted massive sulfide deposits: variations through geologic time and with tectonic setting. Econ. Geol. 105, 571–591.
Inverno, C., Solomon, M., 2001. New mineralogical and fluid inclusion evidence from the Feitais stockwork, Aljustrel, Iberian Pyrite Belt, Portugal [ext. abs.]. GEODE Workshop Massive Sulfide Deposits in the Iberian Pyrite Belt: New Advances and Comparison with Equivalent Systems, Aracena, Spain, pp. 28–30.
Jiang, Y.H., Luo, Y., Niu, H.C., Li, N.B., Guo, S.L., Bao, Z.W., Shan, Q., 2013. Study on fluid inclusions from the Luojiahe Cu deposit in Zhongtiaoshan region. Acta Petrol. Sin. 7, 2583–2592 (in Chinese with English abstract).
Katsev, S., Crowe, S.A., 2015. Organic carbon burial efficiencies in sediments: the power law of mineralization revisited. Geology (G36626-1).
Knauth, L.P., 2005. Temperature and salinity history of the Precambrian ocean: implications for the course of microbial evolution. Palaeogeogr. Palaeoclimatol. Palaeoecol. 219, 53–69.

Lao, K., 1982. Thermo-geochimie appliquée aux inclusion fluides reliées au gisement volcanogene Archean de Millenbach, Rouyn-Noranda, Quebec: Unpublished Ph.D. thesis, Montreal, Quebec, Ecole Polytechnique, pp. 332.
Lecumberri-Sanchez, P., Steele-MacInnis, M., Bodnar, R.J., 2012. A numerical model to estimate trapping conditions of fluid inclusions that homogenize by halite disappearance. Geochim Cosmochim Acta 92, 14–22.
Li, J., Kusky, T., Niu, X., Feng, J., Polat, A., 2004. Neoarchean massive sulfide of Wutai Mountain, North China: a black smoker chimney and mound complex within 2.50 Ga-old oceanic crust. Precambrian ophiolites and related rocks. Developments in Precambrian Geology. 13, pp. 339–361.
Li, J.Y., 1986. Metallogenetic research of a new type Cu deposit in Zhongtiaoshan. Geol. Explor. 17–23 (in Chinese).
Lilley, M., Butterfield, D., Olson, E., Lupton, J., Macko, S., McDuff, R., 1993. Anomalous CH_4 and NH_4+ concentrations at an unsedimented mid-ocean-ridge hydrothermal system. Nature 364, 45–47.
Liu, C., Zhao, G., Sun, M., Zhang, J., Yin, C., 2012. U–Pb geochronology and Hf isotope geochemistry of detrital zircons from the Zhongtiao Complex: constraints on the tectonic evolution of the Trans-North China Orogen. Precambrian Res. 222–223, 159–172.
Liu, H.B., Jin, G.S., Li, J.J., Han, J., Zhang, J.F., Zhang, J., Zhong, F.W., Guo, D.Q., 2013. Determination of stable isotope composition in uranium geological samples. World Nucl. Geosci. 30, 174–179 (in Chinese with English abstract).
Longstaffe, F.J., 1989. Stable isotopes as tracers in clastic diagenesis. In: Hutcheon, I.E. (Ed.), Short Course in Burial Diagenesis. Mineral Association of Canada Short Course, pp. 201–284.
Lowe, D.R., Byerly, G.R., 2003. Ironstone pods in the Archean Barberton greenstone belt, South Africa: Earth's oldest seafloor hydrothermal vents reinterpreted as Quaternary subaerial springs. Geology 31, 909–912.
Lu, H.Z., Fan, H.R., Ni, P., Ou, G.X., Shen, Q., Zhang, W.H., 2004. Fluid Inclusion. Science Press, Beijing, pp. 406–419 (in Chinese).
Marshall, B., Giles, A., Hagemann, S., 2000. Fluid inclusions in metamorphosed and synmetamorphic (including metamorphogenic) base and precious metal deposits: indicators of ore-forming conditions and/or ore-modifying histories. Metamorphosed and Metamorphogenic Ore Deposits Rev Econ Geol. 11, pp. 119–148.
Marshall, B., Gilligan, L., 1993. Remobilization, syn-tectonic processes and massive sulfide deposits. Ore Geol. Rev. 8, 39–64.
McCollom, T.M., 2000. Geochemical constraints on primary productivity in submarine hydrothermal vent plumes. Deep-Sea Res. I Oceanogr. Res. Pap. 47, 85–101.
McGowan, R.R., Roberts, S., Foster, R.P., Boyce, A.J., Coller, D., 2003. Origin of the copper-cobalt deposits of the Zambian Copperbelt: An epigenetic view from Nchanga. Geology 31, 497–500.
Mercier-Langevin, P., Gibson, H.L., Hannington, M.D., Goutier, J., Monecke, T., Dubé, B., et al., 2014. A special issue on Archean magmatism, volcanism, and ore deposits: part 2. Volcanogenic massive sulfide deposits preface. Econ. Geol. 109, 1–9.
Mojzsis, S.J., Arrhenius, G., McKeegan, K., Harrison, T., Nutman, A., Friend, C., 1996. Evidence for life on Earth before 3,800 million years ago. Nature 55–59.
Moura, A., 2005. Fluids from the Neves Corvo massive sulfide ores, Iberian pyrite belt, Portugal. Chem. Geol. 223, 153–169.
Naden, J., Shepherd, T.J., 1989. Role of methane and carbon dioxide in gold deposition. Nature 342, 793–795.
Naumov, V., Khakimov, A., Khodakovskiy, I., 1974. Solubility of carbon dioxide in concentrated chloride solutions at high temperatures and pressures. Geochem. Int. 11, 31–41.
Niu, X.L., Li, J.H., Feng, J., 2009. Origin of the Neoarchean massive sulfide deposits in Wutaishan Mt: an indication for the submarine exhalation from the microstructures. Adv. Earth Sci. 9, 1009–1014 (in Chinese).
Oakes, C.S., Bodnar, R.J., Simonson, J.M., 1990. The system NaCl-$CaCl_2$-H_2O: I. The ice liquidus at 1 atm total pressure. Geochim. Cosmochim. Acta 54, 603–610.
Ohmoto, H., Mizukami, M., Drummond, S., Eldridge, C., Pisutha-Arnond, V., Lenagh, T., 1983. Chemical processes of Kuroko formation. Econ. Geol. Monogr. 5, 570–604.
O'Neil, J.R., Clayton, R.N., Mayeda, T.K., 1969. Oxygen isotope fractionation in divalent metal carbonates. J. Chem. Phys. 51, 5547.
Polat, A., Kusky, T., Li, J., Fryer, B., Kerrich, R., Patrick, K., 2005. Geochemistry of Neoarchean (ca. 2.55–2.50 Ga) volcanic and ophiolitic rocks in the Wutaishan greenstone belt, central orogenic belt, North China craton: implications for geodynamic setting and continental growth. Geol. Soc. Am. Bull. 117, 1387–1399.
Polito, P., Bone, Y., Clarke, J., Mernagh, T., 2001. Compositional zoning of fluid inclusions in the Archaean Junction gold deposit, Western Australia: a process of fluid–wall-rock interaction? Aust. J. Earth Sci. 48, 833–855.
Ramboz, C., Schnapper, D., Dubessy, J., 1985. The P-V-T-X-fO_2 evolution of H_2O-CH_4-CO_2-bearing fluid in a wolframite vein: reconstruction from fluid inclusion studies. Geochim. Cosmochim. Acta 49, 205–219.
Rasmussen, B., 2000. Filamentous microfossils in a 3,235-million-year-old volcanogenic massive sulfide deposit. Nature 405, 676–679.
Ripley, E., Ohmoto, H., 1977. Mineralogic, sulfur isotope, and fluid inclusion studies of the stratabound Cu deposits at the Raul mine, Peru. Econ. Geol. 72, 1017–1041.
Roedder, E., 1984. Fluid inclusions. Rev. Mineral. 12, 646.
Rosing, M.T., 1999. ^{13}C-depleted carbon microparticles in >3700-Ma sea-floor sedimentary rocks from West Greenland. Science 283, 674–676.
Schidlowski, M., 2001. Carbon isotopes as biogeochemical recorders of life over 3.8 Ga of Earth history: evolution of a concept. Precambrian Res. 106, 117–134.
Seewald, J.S., Reeves, E.P., Bach, W., Saccocia, P.J., Craddock, P.R., Shanks, W.C., et al., 2015. Submarine venting of magmatic volatiles in the Eastern Manus Basin, Papua New Guinea. Geochim. Cosmochim. Acta 163, 178–199.
Seyfried, W., Pester, N.J., Tutolo, B.M., Ding, K., 2015. The Lost City hydrothermal system: constraints imposed by vent fluid chemistry and reaction path models on subseafloor heat and mass transfer processes. Geochim. Cosmochim. Acta 163, 59–79.
Shanks, W., 2001. Stable isotopes in seafloor hydrothermal systems: vent fluids, hydrothermal deposits, hydrothermal alteration, and microbial processes. Rev. Mineral. Geochem. 43, 469–525.
Shen, P., Shen, Y., Wang, J., Zhu, H., Wang, L., Meng, L., 2010. Methane-rich fluid evolution of the Baogutu porphyry Cu–Mo–Au deposit, Xinjiang, NW China. Chem. Geol. 275, 78–98.
Spooner, E., Bray, C., 1977. Hydrothermal fluids of seawater salinity in ophiolitic sulfide ore deposits in Cyprus. Nature 266, 808–812.
Springer, J.S., 1985. Carbon in Archean rocks of the Abitibi belt (Ontario-Quebec) and its relation to gold distribution. Can. J. Earth Sci. 22, 1945–1951.
Staudigel, H., 2014. Chemical fluxes from hydrothermal alteration of the oceanic crust. Treatise on Geochemistry. Elsevier, Oxford, pp. 583–606.
Steele-MacInnis, M., Bodnar, R., Naden, J., 2011. Numerical model to determine the composition of H_2O–NaCl–$CaCl_2$ fluid inclusions based on microthermometric and microanalytical data. Geochim. Cosmochim. Acta 75, 21–40.
Sun, J.Y., Ji, S.K., Zhen, Y.Q., 1995. The Cu Deposits in the Zhongtiao Rift. 1th ed. Geological Publishing House, Beijing, pp. 84–140 (in Chinese).
Sun, D.Z., Hu, W.X., 1993. Precambrian Geochronology, Chronotectonic Framework and Model of Chronocrustal Structure of the Zhongtiao Mountains. 1th ed. Geological Publishing House, Beijing, pp. 1–102 (in Chinese).
Takenouchi, S., Kennedy, G.C., 1964. The binary system H_2O-CO_2 at high temperatures and pressures. Am. J. Sci. 262, 1055–1074.
Taylor, H., 1974. The application of oxygen and hydrogen isotope studies to problems of hydrothermal alteration and ore deposition. Econ. Geol. 69, 843–883.
Tornos, F., Peter, J.M., Allen, R., Conde, C., 2015. Controls on the siting and style of volcanogenic massive sulfide deposits. Ore Geol. Rev. 68, 142–163.
Ueno, Y., 2014. Earth Science. Coping with low ocean sulfate. Science 346, 703–704.
van Zuilen, M.A., Lepland, A., Teranes, J., Finarelli, J., Wahlen, M., Arrhenius, G., 2003. Graphite and carbonates in the 3.8 Ga old Isua supracrustal belt, southern West Greenland. Precambrian Res. 126, 331–348.
Vanko, D.A., 1988. Temperature, pressure, and composition of hydrothermal fluids, with their bearing on the magnitude of tectonic uplift at mid-ocean ridges, inferred from fluid inclusions in oceanic layer 3 rocks. J. Geophys. Res. Solid Earth 93, 1978–2012 (4595–4611).
Westall, F., Campbell, K.A., Breheret, J.G., Foucher, F., Gautret, P., Hubert, A., et al., 2015. Archean (3.33 Ga) microbe-sediment systems were diverse and flourished in a hydrothermal context. Geology 43, 615–618.
Xu, J.H., Hart, C.J.R., Wang, L.L., Chu, H.X., Lin, L.H., Wei, X.F., 2011. Carbonic fluid overprints in volcanogenic massive sulfide deposits: examples from the Kelan Volcanosedimentary Basin, Altaides, China. Econ. Geol. 106, 145–158.
Xu, Q.L., 2010. Study on the Geological Characteristics and Ore Genesis of Tongkuangyu Cu Deposit in the Zhongtiaoshan Mountains, Shanxi Province (Master thesis) Jilin University, pp. 59–71 (in Chinese with English abstract).
Yang, K., Scott, S.D., 1996. Possible contribution of a metal-rich magmatic fluid to a seafloor hydrothermal system. Nature 383, 420–423.
Yang, K., Scott, S.D., 2005. Magmatic sources of volatiles and metals for volcanogenic massive sulfide deposits on modern and ancient seafloors: evidence from melt inclusions. Mineral Deposit Research: Meeting the Global Challenge. Springer, pp. 715–718.
Zaw, K., Huston, D., Large, R., Mernagh, T., Hoffmann, C., 1994. Microthermometry and geochemistry of fluid inclusions from the Tennant Creek gold-Cu deposits: implications for ore deposition and exploration. Mineral. Deposita 29, 288–300.
Zhao, G.C., Cawood, P.A., Wilde, S.A., Sun, M., 2002a. Review of global 2.1–1.8 Ga orogens: implications for a pre-Rodinia supercontinent. Earth Sci. Rev. 59, 125–162.
Zhao, G., Wilde, S.A., Cawood, P.A., Sun, M., 2001. Archean blocks and their boundaries in the North China Craton: lithological, geochemical, structural and P–T path constraints and tectonic evolution. Precambrian Res. 107, 45–73.
Zhao, G., Wilde, S.A., Sun, M., Guo, J., Kröner, A., Li, S., et al., 2008. SHRIMP U–Pb zircon geochronology of the Huai'an Complex: constraints on late Archean to Paleoproterozoic magmatic and metamorphic events in the Trans-North China Orogen. Am. J. Sci. 308, 270–303.
Zhao, T.-P., Zhou, M.-F., Zhai, M., Xia, B., 2002b. Paleoproterozoic rift-related volcanism of the Xiong'er Group, North China craton: implications for the breakup of Columbia. Int. Geol. Rev. 44, 336–351.
Zhao, Y., Niu, H.C., Jiang, Y.H., Li, N.B., 2016. Petrogenesis of Late Neoarchean (~2.5 Ga) Na-rich and K-rich Granitoids From the Southern North China Craton: Implications for Lithospheric Delamination, in Writing.
Zhen, Y.Q., Wu, J.F., 2007. Triplet assemblage of ore-bearing strata of Luojiahe Cu deposit in Zhongtiaoshan region. J. Guilin Univ. Technol. 3, 310–319 (in Chinese).
Zhen, Y.Q., Du, J.S., Liu, L.L., 1993. The Zhongtiao Rift Zone and the Luojiahe Cu Deposit. China University of Geosciences Press, Wuhan (in Chinese).
Zhen, Y.Q., Xi, Z.R., 1990. Geochemical features of RE-elements in the Luojiahe Cu-deposit in Zhongtiao Mountain. Geol. Explor. 15–21 (in Chinese).